Utrecht University

Geological constraints on tidal dissipation in the Messinian

An XRF record of climate variability from Gavdos Island (Greece)

30/04/2021

MSc Thesis: J.H.P.C. Mandemaker
Student number: 5740398
Email: j.h.p.c.mandemaker@students.uu.nl

Supervisors:
Prof. Dr. L.J. Lourens
Dr. F.J. Hilgen

Department of Earth Sciences
Faculty of Geoscience
Utrecht University

Table of contents

Cover photo: The Metochia section on Gavdos Island with the protruding diatomites clearly visible.

Online Gea magazine March 2020**,** by: *Annemieke van Roekel - redactie.vanroekel@gea-geologie.nl*

Abstract

The climatic response to astronomical forcing in sedimentary archives provides insights into the effect of tidal dissipation (Td) and dynamical ellipticity (dE) on the astronomical solutions. The astronomical solutions are used to compute insolation and orbital target curves for paleoclimatic research. It is therefore most fundamental to understand their role as phase relations between astronomical forcing and climate response can only be accurately calculated when the Td and dE parameters are known. In this thesis, I determine the average values of tidal dissipation for the Messinian using an XRF record from the sapropel-bearing Metochia section (Gavdos, Greece), using the assumption of a direct response of sapropel formation to insolation. An exceptional palaeoclimate proxy (Fe/Ti) that records humid as well as arid conditions related to the African monsoon is compared with the insolation record of an astronomical solution (La2001) with varying values for the tidal dissipation. It is found that the optimum fit between the proxy data and astronomical model is obtained for the $La2001_{(1,1.1)}$ solution. This value is, however, statically indistinguishable to that of the $La2001_{(1,1.2)}$ and $La2001_{(1,1)}$ solutions. The use of the $La2001_{(1,1.1)}$ solution implies a -2.12 ± 0.03 kyr phase lag for precession and a -2.04 ± for 0.07 kyr for obliquity compared to the commonly used La2004 solution. An additional ~3.5 kyr lag to precession minima is quantified for the diatomites of the Metochia section, which should be taken into account when applying astronomical tuning to other Mediterranean diatomites.

1. Introduction

Our understanding of the phase relation between solar insolation and Earth's climate has always been of major interest in paleoclimatology. In particular, the Earth's climatic response in paleoclimate archives allows for the discrimination between cause and effect in unravelling fundamental processes controlling Earth's history as well as the rates of change in the geological past. Essential to the determination of such phase relations are accurate and precise knowledge of geological time. For the Pleistocene and Pliocene, the geological time scales have an unprecedented accuracy, precision, and resolution, as portrayed by the Astronomically Tuned Neogene Time Scales 2004 and 2012 (ATNTS; Gradstein et al., 2004, 2012; Hilgen et al., 2012; Lourens et al., 2004). In contrast, high-resolution time scales for the Neogene often rely on inter-calibrations of orbital tuning with magneto- and biostratigraphy, $^{40}Ar/^{39}Ar$ and/or $^{238}U/^{206}Pb$ dating, while uncertainties in radioisotopic dating, and, in the computations of Earth's orbital parameters have obstructed the construction of a reliable time scale beyond 40 Ma (Westerhold et al., 2012). An inter-calibration of astronomically dated tephra layers and intercalated $^{40}Ar/^{39}Ar$-dated sanidine crystals from the Messinian Melilla Basin in Morocco was used to improve the age of Fish Canyon sanidine; the most widely used standard in $^{40}Ar/^{39}Ar$ geochronology (Kuiper et al., 2008). Uncertainties in the astronomical ages of the radio-isotopically dated tephra horizons, and therefore in the age of the Fish Canyon sanidine, could originate from the assumption that the lag between the orbital forcing and sedimentary expression is zero. Although the phase relation of diatomites to orbital forcing is known, it has not yet been directly quantified (Hilgen and Krijgsman, 1999).

To improve our understanding of Earth's climatic response to orbital forcing as well as to obtain a tuned time scale with the highest accuracy and precision, it is imperative to constrain the effect of changing values of tidal dissipation (Td) and dynamical ellipticity (dE) in the astronomical solution on precession and obliquity. Td and dE are both considered in the calculation of the precession constant and therefore have a direct effect on precession and obliquity frequencies. In the astronomical solution, the present rate of change in the motion of the Moon is used to calculate Td and the associated change in precession and obliquity frequencies (Laskar et al., 1993). However, if the observed present-day tidal dissipation rates are representative of the past, the moon must be younger than 1500 Ma (Hansen, 1982; Sonett et al., 1996), whereas it is known that the Moon formed in the early Solar System (~4500 Ma; e.g.: Lee et al., 1997; Barboni et al., 2017). A lower recession rate of the moon must be tied to a weaker tidal dissipation; hence, it can be stated that periods of weak tidal dissipation must have existed in the geological past (Williams, 2000).

Astronomical solutions such as La90, La93, La2001, La2004, and $La2010_{a-d}$ are analytical solutions that numerically integrate information of all eight planets of the solar system (Laskar, 1990; Laskar et al., 1993; Laskar, 2001; Laskar et al., 2004, 2011). The La2004 solution uses a direct integration of the gravitational equations for the orbital motion and improves the dissipative contributions compared to previous solutions, in particular in the evolution of the Earth-Moon System. Furthermore, the La2004 solution uses more precise initial conditions, while the $La2010_{a-d}$ solutions focus more on the orbital solution of the Earth and more specifically on the long period terms in the eccentricity (Laskar et al., 2004; 2011). The precessional motion and obliquity evolution of the spin axis of the Earth thus remain identical for the La2004 and $La2010_{a-d}$ solutions, and by doing so, leave the uncertainties

regarding the evolution of tidal dissipation in the Earth-Moon system yet unresolved. Although changing values of Td and dE in the astronomical solution cannot be directly verified by astronomical theory, a detailed comparison with paleoclimate data can put constraints on values for Td and dE (Pälike and Shackleton, 2000; Lourens et al., 2001; Hüsing et al., 2007; Zeeden et al., 2014).

For the late Pleistocene, the effect of Td and dE on precession and obliquity is almost negligible, but numerical models have shown that the value for Td indeed changes nonlinearly further back in time and results in uncertainties in the precession and obliquity frequencies (Green and Huber, 2013; Green et al., 2017). However, Pälike and Shackleton (2000) demonstrated that the present-day values of Td and dE in the La93 solution (Laskar et al., 1993) between 0 and 11.5 Ma, and between 17.5 and 24 Ma resulted in a good match with the precession-obliquity interference patterns in the high-resolution proxy records from Ocean Drilling Program (ODP) Site 926 (Ceara Rise, western equatorial Atlantic). This is in agreement with the findings of Lourens et al. (2001), who used the Ti/Al elemental ratio as a proxy for relative aridity from ODP Site 967. Lourens et al. (2001) concluded that the present-day values for Td and dE in the La90 solution (Laskar, 1990) resulted in a good fit with the paleoclimatic record between 2.4 and 2.9 Ma. Despite that the La90 solution with a Td parameter of 0.5 provided even more consistent results with the geological record, a Td of ~1 was suggested as these options were considered statistically indistinguishable (Lourens et al., 2001).

More recently, Zeeden et al. (2014) demonstrated using quantitative colour records from the Monte dei Corvi section (northern Italy) that the tidal dissipation rate between 11.5–12.3 Ma was either at least within 10%, or, 40% of the present-day value, with the lower estimate obtained by shifting the precession a whole cycle. Hüsing et al. (2007) even concluded that a tidal dissipation rate of 20% higher than the present-day value is preferred for time intervals older than 10.2 Ma. Furthermore, the Td value of 40% from Zeeden et al. (2014) is supported by a numerical tidal model, which suggested that the tidal dissipation rates during the Cenozoic were weaker than at present, except for the glacial states over the last 2 Ma (Green et al., 2017). Consequently, it remains important to obtain more high-resolution records that allow for a precise quantification of Td and/or dE values, which is fundamental for determining phase relations between insolation forcing, climate response, and the registration in the paleoclimate archives.

In this thesis, I will present an X-Ray Fluorescence (XRF) record of cyclic patterns related to precession-obliquity interference in the sapropel-bearing succession of the Metochia section (Gavdos) to investigate the effect of Td in the Messinian (dE will be kept fixed at the present-day value). The effect of Td has previously been investigated for the Serravallian and Tortonian (Hüsing et al., 2007; Zeeden et al., 2014), but a quantitative study has not yet been undertaken for (part of) the Messinian. Results of this study will be compared with the nearby Ayos Miron section (Crete), and, will be used to determine the phase relation of the diatomites that overly the sapropelic layers of the Metochia section. The phase relation between insolation forcing and diatomite formation could have implications for the astronomical tuning of diatomites in the Mediterranean area and, therefore, for the calibration of $^{40}Ar/^{39}Ar$ dating techniques (Kuiper et al., 2008). A reliable inter-calibration is crucial for

the consistency and incorporation in the standard Geological Time Scale (Kuiper et al., 2008; Rivera et al., 2011).

2. Geological setting and section

The pre-evaporitic Metochia D section is located on the island of Gavdos in the eastern Mediterranean Sea (Greece; Fig. 1; *cover photo*). The section provides a unique Messinian succession as safety regulations do not allow drilling through the Messinian abyssal evaporites and can, therefore, only be studied on land. Benthic foraminiferal assemblages in the Metochia section are characteristic of an outer shelf to slope environment in a restricted basin (Drinia et al., 2007). The tectonically uplifted deep marine sediments were deposited at a water depth of 1000–1200 m during the late Miocene (van Hinsbergen and Meulenkamp, 2006), and consist of cyclic tripartite alternations that are composed of a sapropel at the base, followed by a prominent diatomite, and a homogeneous marl layer on top (Fig. 1; Krijgsman et al., 1995, 1999).

Drinia et al. (2007) consider that the Metochia section does not contain true sapropels and consists of alternating clayey diatomites, white diatomites and diatomaceous laminated marls. However, in this thesis these layers are considered as homogenous marls, diatomites, and sapropels. Sapropels are organic-rich layers that occur widespread throughout the Mediterranean Neogene. The formation of Mediterranean sapropels has been attributed to enhanced runoff at precession minima and has been associated with enhanced summer monsoonal rainfall of North African origin, flowing into the Mediterranean Sea via the Nile river (Rossignol-Strick, 1985), the Chad-Eosahabi catchment area (Griffin, 2002, 2006), and short-lived wadi systems and other extinct rivers during the late Miocene (Coulthard et al.,

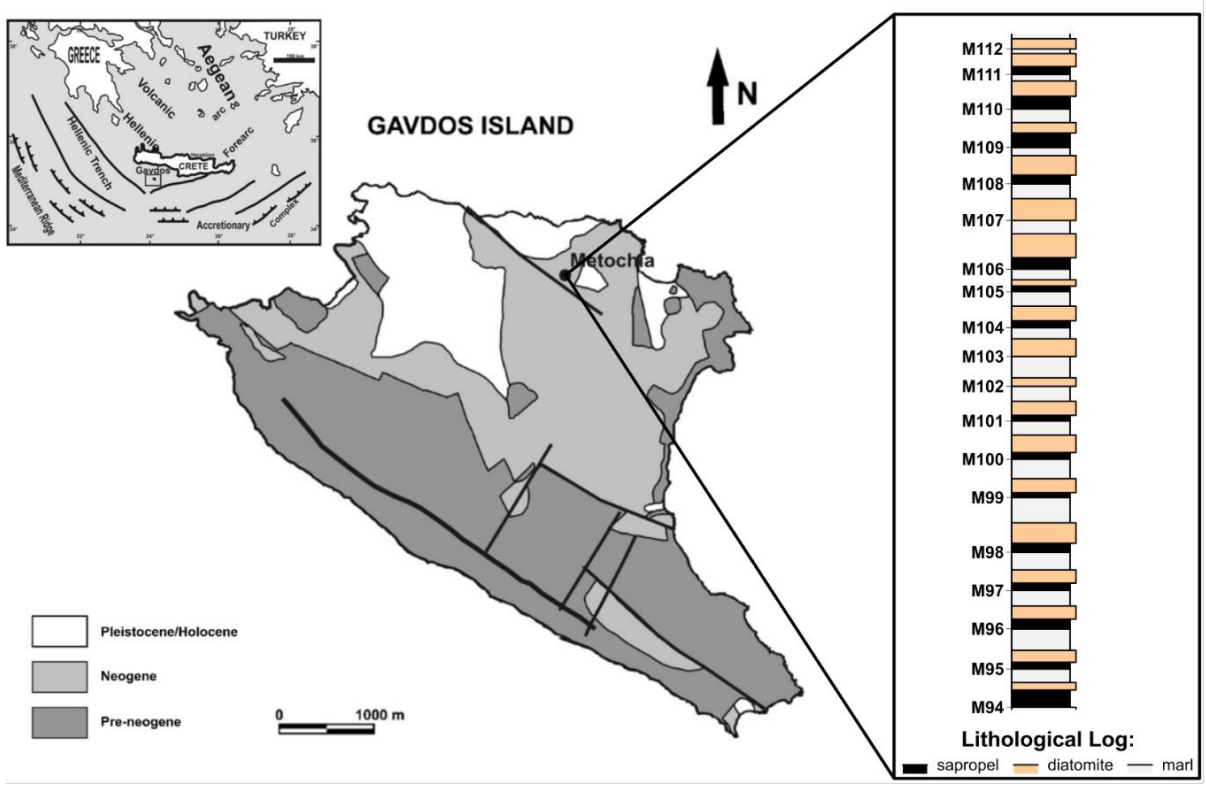

Fig. 1. Simplified geological map of the Gavdos Island indicating the location of the pre-evaporitic sequence of the Metochia section and its lithological log with Metochia cycle numbers (modified from: Drinia et al., 2007).

2013; Ghoneim et al., 2012; Paillou et al., 2009, 2012). It also has been demonstrated that three well-developed 10 Ma old sapropels from the Metochia section are the result of precession induced dry–wet oscillations in the Mediterranean climate (Schenau et al., 1999). An in-phase relation between insolation forcing and the climatic response in sapropels is essential for this study but can be assumed for both the precession and the obliquity signals, as both have been shown to relate to monsoon-induced variations in runoff into the Mediterranean Sea (Tuenter et al., 2003; Bosmans et al., 2015; Marzocchi et al., 2019; De Boer et al., 2021).

Furthermore, the characteristic sedimentary cycle patterns allowed for the calibration to the 65°N summer insolation record of Laskar (1990), and hence, provided the Messinian age for the Metochia D section (Hilgen et al., 1995). For this study, however, revised sapropel ages following the improved orbital solution of Laskar et al. (2004) are initially used (*see section 3.4)*, resulting in an age of 6.71 – 6.39 Ma for the studied section. These updates in the La2004 solution result on average in a 2.5 ka shift to younger ages. The contiguous cyclicity of the Metochia sediments moreover has resulted in the extension of the astronomical polarity timescale from 5 to 10 Ma, forming a fundamental component of the stratigraphic framework for the Mediterranean Upper Miocene (Hilgen et al., 1995).

3. Material and methods

For this study, a 7.46 meter section (89.92 m - 97.38 m; Fig. 1) was sampled on average every 4.8 centimetres on average, resulting in an average temporal resolution of 2.08 kyr. The 154 sediment samples from the Metochia D section had previously been collected during fieldwork and were stored at the Utrecht University. Sandstones and turbiditic layers were excluded from further analyses.

3.1 Sample preparation

The samples were prepared for further analyses using the Herzog HP-MA: automatic pulverizing mill. A tungsten carbide grinding vessel was used for the grinding of sample material. After pulverizing the grinding vessel was automatically emptied and the ground material was made available at the discharge point. The use of different cleaning functions, namely compressed air and wet cleaning, allowed sufficient material removal, and cross-contamination was reduced to a low ppm-level. After homogenization, the samples were transferred to 60 ml polypropylene (PP) containers.

3.2 Thermogravimetric analysis

Thermogravimetric analysis (TGA) was used to remove all residual moisture, oxidize organic matter and carbonates, and to determine the loss on ignition (LOI). This was achieved by heating the samples to elevated temperatures (105 °C, 450 °C, 550 °C, 800 °C, and 1000 °C) until the weight of the sample stabilized. The LECO TGA 701 can accept 19 samples and one calibration standard. Crucibles were weighed in a carousel, after which at least 3.0 grams of sample were added. The mass of each sample was then measured automatically. The accuracy of the measurement is determined by the scale in the TGA (± 0.0001 grams). Expressed as a percentage of up to 3 grams of dry weight at 105 °C, it

results in a reporting limit of 0.01% weight loss at 105 °C, 450 °C, 550 °C, 800 °C and 1000 °C in the sediment samples.

3.3 X-Ray Fluorescence analysis

Bulk concentrations of major elements were determined by X-Ray Fluorescence (XRF). After the TGA, 600 mg of the roasted sample was carefully weighed, placed in platinum crucibles, and mixed with 6000 mg of pre-fused flux: ICPH, Fluomix 6516 LiI; 66% Lithium Tetraborate ($Li_2B_4O_7$), 34% Lithium Metaborate ($LiBO_2$), with an addition of 0.5% Lithium Iodide (LiI) to prevent sticking of the molten sample to the crucibles. The mixture was then fused into glass pearls (ø 39 mm) at 1200 °C using the Herzog HAG-S fusion system. The resulting glass pearls were then analysed for the elements Al, Ba, Ca, Cr, Fe, K, Mg, Mn, Ni, P, Si, Sr, Ti and, Zr, by an ARL Perfom'X Sequential X-Ray Fluorescence (XRF) Spectrometer. Analytical precision was determined by parallel analysis of an international standard (ISE 921) to be better than <1% for Al, Fe, Si, and, Ti.

3.4 Estimates for the calcium carbonate and organic matter content

The calcium carbonate ($CaCO_3$) content was estimated in two different semi-quantitative ways; based on the assumption that no other CaO-rich phases are present in the sediments, and CaO is thus only present as calcite, using the formula: $CaCO_3$ = CaO x 1.7848 (Wehausen and Brumsack, 2002), and, by using a calculation based on the weight loss obtained after samples were heated from 550 °C to 800 °C multiplied with 100/44 (TGA regulation from Utrecht University and TNO-NITG, unpublished). The organic carbon content (C_{org}) was estimated in a similar semi-quantitative way as the weight loss obtained after heating the sediment material to 450 °C and 550 °C can be regarded as an estimate of the organic carbon content.

3.5 Cross spectral analysis

For the computation of average Td values (dE is kept constant in this study) for the 6.71 – 6.39 Ma time interval, it was first needed to determine the midpoints of maxima and minima in the proxy record. Preferably, a proxy record that provides a direct and linear relation to precession/monsoon-induced variations was used (e.g., Ti/Al: Lourens et al., 2001; Fe/Ti: this study). Hence, midpoints of maxima/minima in the 1-kyr interpolated Fe/Ti record were correlated to consequent midpoints of extremes in the 65°N insolation record of the La2001 solutions, which contain different values for Td in steps of 0.1 (relative to the present-day value of 1). This assignment of astronomical ages implied small modifications of the Fe/Ti time series for each solution. Similar to the approach of Zeeden et al. (2014), values for Td were modified in the La2001 solution (J. Laskar, unpublished data, 2001), which allows adjustment of these parameters similar to the Laskar et al. (1993) routine. Despite a small offset in absolute insolation values due to the adopted value for the solar constant, the La2001 and La2004 solutions are nearly identical over the last 15 Ma for present-day values of Td and dE; they are therefore interchangeable and can be directly compared for the time interval used in this study (Fig. 2). Moreover, it must be noted that the choice for the 65°N summer insolation record instead of the 23°N-23°S Summer Inter Tropical Insolation Gradient (SITIG), or, the P - 1/2t (precession minus a half tilt) target curves provide almost identical target curves and therefore do not influence the outcome of

this study (Reichart, 1997; Bosmans et al., 2015; Lourens et al., 1996; Lourens et al., 2001). For the calculation of the precession and obliquity-related time lags between the 65°N insolation curve and the proxy data time series cross-spectral analyses was applied using the Blackman-Tukey method as implemented in the Analyseries software (Paillard et al., 1996). Average frequency bands that correspond to periods of 18–25 and 38–45 kyr were investigated for the phase of precession and obliquity. It has been proposed that the obliquity phase is a reliable indicator of the consistency between the astronomical solution and proxy data as the obliquity phase is more sensitive to Td variations than the coherence (Lourens et al., 2001; Morrow et al., 2012; Zeeden et al., 2014). For the cross-spectral analyses, a Parzen smoothing-window with 150 lags (~50 % of the series) was used, which resulted in a bandwidth of 0.012362. The lower and upper confidence limits at the 97.5% level are given by: $0.399262 < \Delta P\ (97.5\%)/P < 4.937814$ (Figs. 6, 7, and 8). To evaluate the fit of an astronomical solution (using specific Td values) with proxy data, the Pearson correlation coefficient was calculated between the tuned proxy data set and the astronomical target curves. Given that the Fe/Ti record shows a near-linear response to the target curves the Pearson correlation coefficient (Pearson, 1895) was preferred over the Spearman rank correlation, the latter being used by Zeeden et al. (2014) because of the non-linear proxy data.

At last, as is common in the literature, values for Td and dE are here denoted between

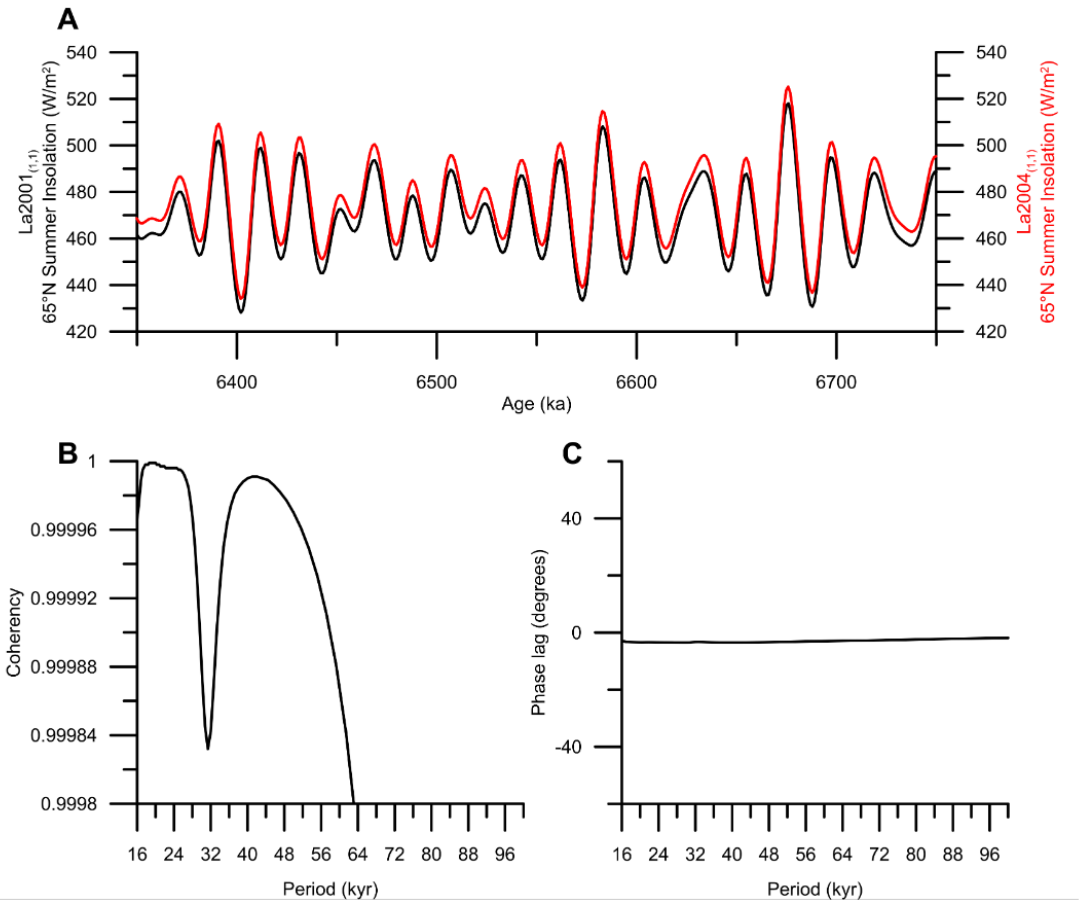

Fig. 2. A) The Laskar2001 (black) and Laskar2004 (red) astronomical solutions with present-day values for Td and dE (Laskar, 2001; 2004). **B**) Coherency spectrum between the time series of the astronomical solutions, and **C)** phase spectrum (degrees) between the time series of the astronomical solutions.

brackets in subscript and as suffix behind the astronomical solution (Fig. 2). In this manner, present-day values are presented as (1,1) and higher or lower values, therefore, represent increased or decreased average values of Td over the considered time interval (e.g., $La2001_{(1,Td)}$, with dE = 1 and varying values for Td).

4. Results

4.1 Bulk sediment geochemistry

The geochemical results of the investigated sediments are shown in figure 3, in which the trends throughout the section are illustrated as element ratios of elemental percentages (%) and parts per million (ppm). To compensate for carbonate dilution the chemical composition of the sediments is presented here on the basis of element/Al ratios. Sedimentary cycles in the lithological log are annotated as M-cycles, with a sapropel at the base, overlain by a diatomite, and a marl layer at the top. Diatomites are also annotated as D-cycles at the right side of the lithological log.

The $CaCO_3$ content, estimated from the CaO-based calculation, is present at markedly low values in most sapropels and especially in the diatomites (Fig. 3a). It displays values of < 30% in diatomite cycles D3, D7, D8, D13, D14, and D15. However, it also reaches

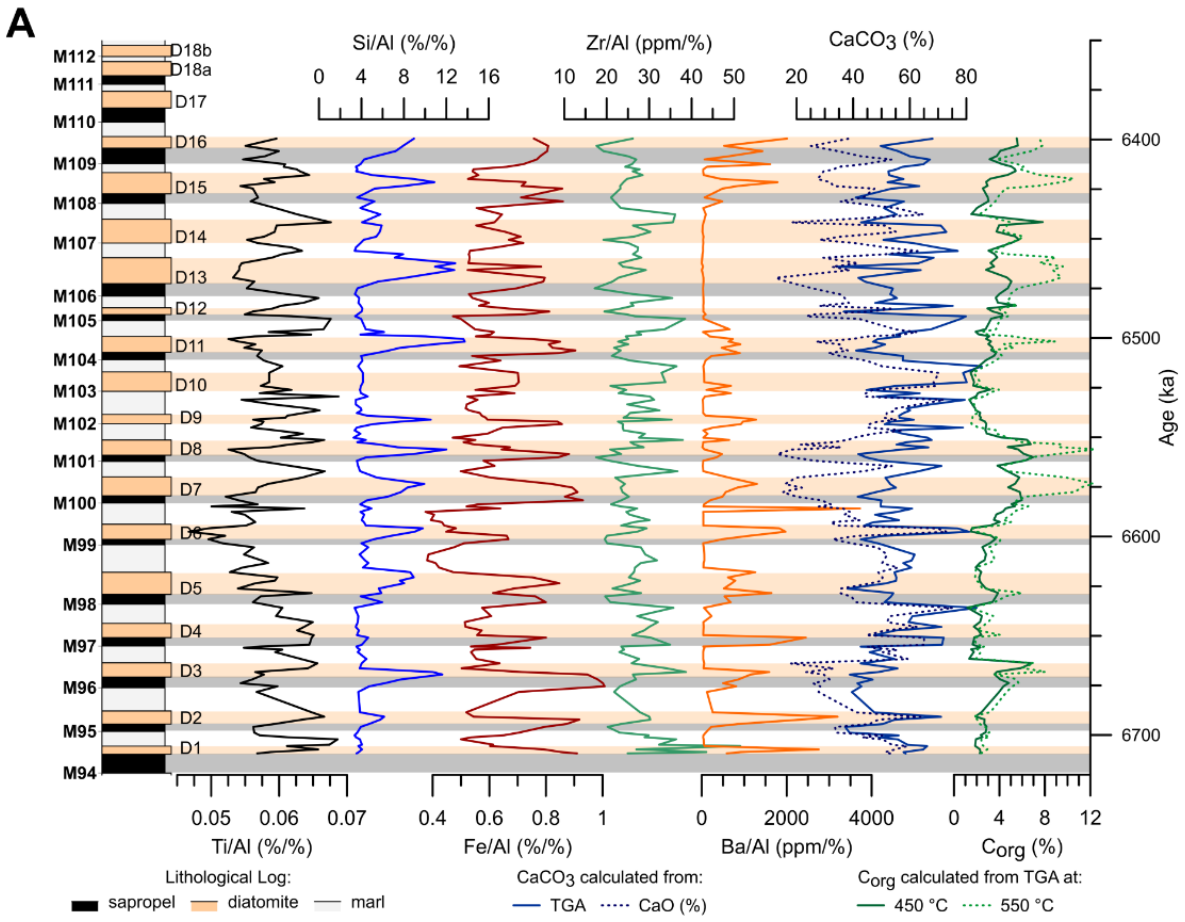

Fig. 3. Elemental ratios, estimated carbonate contents, and estimated organic carbon contents for the Metochia D section plotted on a timescale (6.72 – 6.4 Ma). The lithological log is plotted on the right, with numbered Metochia cycles (M94-M112) plotted on the left (bold) and numbered diatomite cycles (D1 – D18b) on the right. The lithological log is also plotted on the background, where the grey bars represent sapropels, light orange bars represent diatomites, and white bars represent homogenous marls.

over 60% in diatomite cycles D2, D6, D10, as well as in the sapropel of M97. In general, no clear correlation between the different sedimentary layers can be observed. Although almost identical trends occur in the $CaCO_3$ content of the TGA-based estimate, this pattern seems to display less extreme low values. Moreover, this pattern presents a baseline near 40%, whereas maxima in general show relatively lower values. The C_{org} content variations are more closely related to the lithology of the Metochia section when compared to the $CaCO_3$ record (Fig. 3a). The maximum C_{org} content is observed in the diatomites, which show values of 4 - 8%, except for diatomite cycles D2, D4, D9, and D10 that show values lower than 4%. The most extreme values of C_{org} (> 8%) correspond well with the observed low $CaCO_3$ content in diatomites D3, D7, D8, D13, D14, and D15. Although the lowest values for C_{org} are observed in the homogenous marls its C_{org} content often exceeds 2%, which is commonly considered as the limit for classification as sapropels (Ten Haven et al., 1987).

The barium (Ba) content is significantly enriched (>300 ppm; Thomson et al., 1993) within the diatomites and correlates well with the C_{org} pattern, except for cycles M106 and M107 (Fig. 3a). It is likely that the Ba content would have provided a better fit with vanadium (V) for the sapropels as V precipitates under reducing conditions (Thomson et al., 1995; De Lange et al., 2008); however, concentrations of this redox-sensitive element were not measured in this study. Organic matter degradation results in progressive Ba uptake into barite and Ba can therefore serve as an indicator of primary productivity in the surface layers (Dymond, 1992; Thomson et al., 1993). Relative enrichment in Ba in sapropels is well documented for the Pliocene and Pleistocene (Wehausen and Brumsack, 1999; Calvert and Fontugne, 2001), but here the diatomites also show large enrichments, despite that the average Ba/Al ratio is significantly higher in the results of this study (Wehausen and Brumsack, 2000). It should also be noted that Ba can be remobilised diagenetically (Thomson et al., 1993). Such mobilisation can occur during deposition, soon after deposition and/or during a later stage of diagenesis. Ba enrichments cannot be observed in the homogenous marls of this section, except just below the sapropel of cycle M100 (Fig. 3a). This could be interpreted as the result of the mobilisation of Ba from the sapropel above and its reprecipitation in the marl directly beneath, resulting in a “ghost” sapropel. The enrichments in Ba, or productivity, are here clearly related to oceanic opaline production by diatom blooms. This is also clearly reflected in the Si/Al pattern, which shows enrichments in almost all diatomite layers (Fig. 3a). Although the Si/Al ratio is commonly used as proxy for detrital sediment input in sapropels the signal is overprinted by the enhanced input of diatomaceous detritus. The cyclic alternations in the Si/Al record moreover present an alternating thin-thick pattern, which can be most clearly observed at cycles M102 to M108 (Fig. 3a). These patterns are the result of an additional effect of obliquity on insolation, which results in interference patterns that correspond to thin-thick alternations in the Mediterranean sedimentary cycles (Hilgen and Krijgsman, 1999), in which the thicker sapropels and diatomites correspond to the more prominent insolation maxima.

Titanium (Ti) and Zircon (Zr) are known to be enriched in aeolian dust from the Sahara (Guieu and Thomas, 1996; Wehausen and Brumsack, 2000), and both ratios can be used as a dust proxy in the Mediterranean area (Lourens et al., 2001; Jimenez-Espejo et al., 2008;

Rodrigo-Gámiz et al., 2011). Although both the Ti/Al and Zr/Al patterns show relatively low values in the sapropels and diatomites, the Ti/Al pattern reflects the variability in the different sediments most well (Fig. 3a). The Zr/Al record may present a more distorted signal, with high values also occurring at times of sapropel and diatomite deposition. However, it must be noted that high Zr/Al ratios have also been interpreted as indicators of enhanced wind speeds and eolian transport (Calvert and Fontugne, 2001). On the other hand, the Ti/Al record provides a more straightforward pattern. The minimum value for Ti/Al is 0.05 at cycle M99, while maxima do not exceed 0.07. The average Ti/Al value of 0.06 is similar to the averages observed in Pliocene sediments at ODP sites 964 and 969 (Wehausen and Brumsack, 2000). Maxima in Ti/Al values can be interpreted as enhanced dust input during marl deposition, whereas at times of sapropel and diatomite deposition the Ti/Al pattern shows generally low values, indicating an increased fluvial supply of Al-rich elements and a decreased input of Ti-rich aeolian material (Wehausen and Brumsack, 2000; Lourens et al., 2001). This pattern holds for almost all cycles, except it is less evident for cycle M98.

Geochemical alternations related to changes in lithology are best reflected in the Fe/Al record (Fig. 3a). Each sapropel-diatomite succession is marked by high Fe/Al values, whereas each marl layer is marked by low Fe/Al values (0.4-0.55). The Messinian Metochia sediments contain (almost) identical average Fe/Al ratios (0.7) as the Pliocene sediments from ODP sites 966, 967, and 969 (Fe/Al: 0.67 - 0.71; Wehausen and Brumsack, 2000). The maximum value of Fe/Al reaches 1.0 at cycle M96, whereas two minima reach

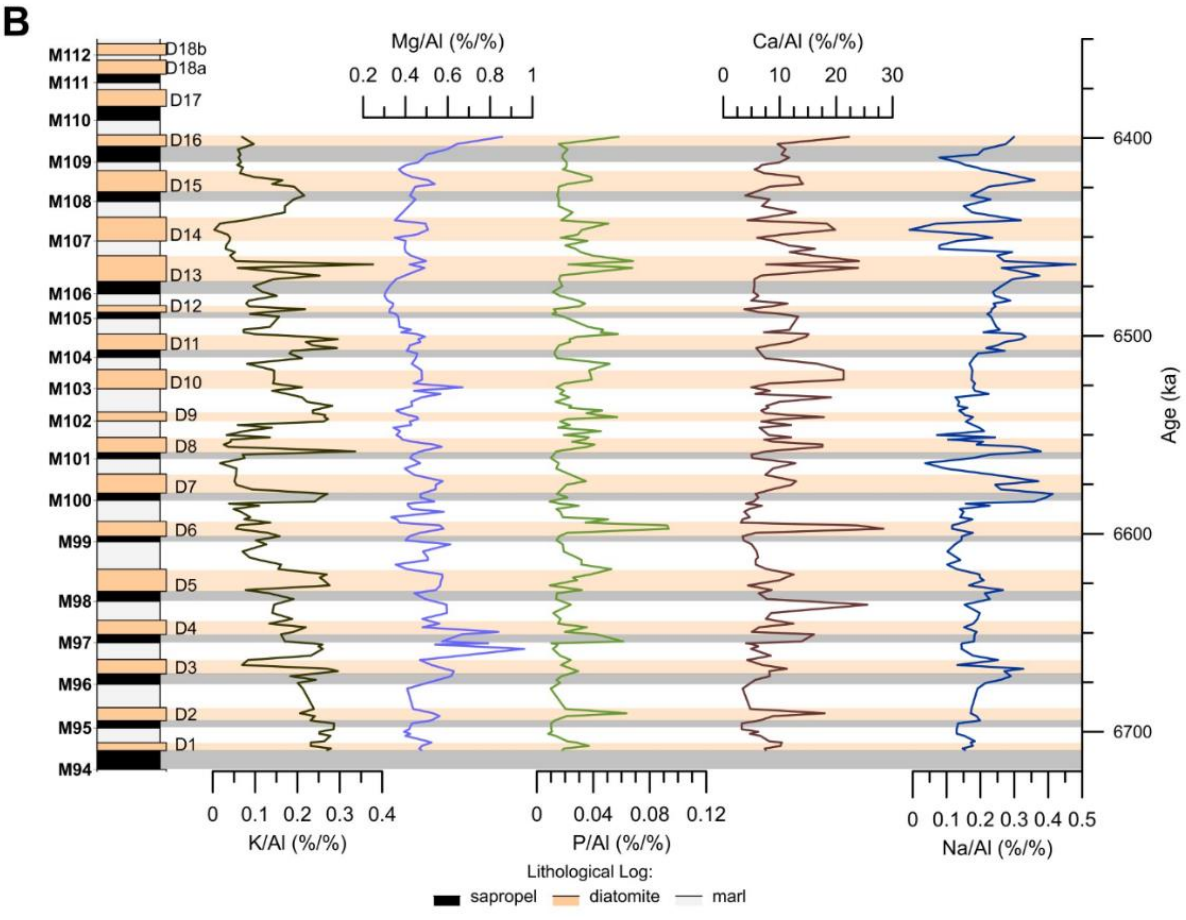

Figure 3 *(continued)*

below 0.4 in the homogenous marls at cycles M98 and M99 (Fig. 3a). Furthermore, two large-scale clusters of cycles are observed that encompass cycles M95, M96, and M97, as well as cycles M101, M102, and M103, which are most likely related to eccentricity maxima. Similar to the Si/Al record, the Fe/Al record shows moreover an alternating thin-thick pattern related to the precession-obliquity interference (Hilgen and Krijgsman, 1999). Enrichments in the Fe/Al ratio could originate from the detrital input and/or the formation of iron sulphide minerals, especially pyrite (FeS_2), that are formed under sulphate-reducing conditions and during the degradation of organic matter (Nijenhuis et al., 1996; Wehausen and Brumsack, 2000; Calvert and Fontugne, 2001). These conditions appear to be well reflected in the Fe/Al pattern and support the idea that sapropels are formed under anoxic conditions (Rossignol-Strick, 1985). Fe/Al peaks even extend into the diatomites, or even when a sapropel is missing, high Fe/Al ratios are observed in the diatomites (diatomite cycles D9, D10, and D14). It can moreover be observed that the transition between sapropels and diatomites is often marked by a decrease in Fe/Al values at cycles M97, M98, M100, M101, M104, and M106.

The P/Al ratio has previously been used as a proxy to assess paleoproductivity in the Pleistocene (Latimer and Filippelli, 2001; Calvert and Pedersen, 2007) and the Early Cenozoic (Latimer and Filippelli, 2002). Although Latimer and Filippelli (2001, 2002) use the P/Ti ratio, the P/Al ratio used here does not result in significant differences for the results of this study. The correspondence between the P/Al, Si/Al, and Ba/Al ratios is strong (Fig. 3b) and supports the suggestion that enrichments in these proxies are related to enhanced productivity by diatom blooms. For the Metochia sediments, the average P/Al ratio (~0.025)

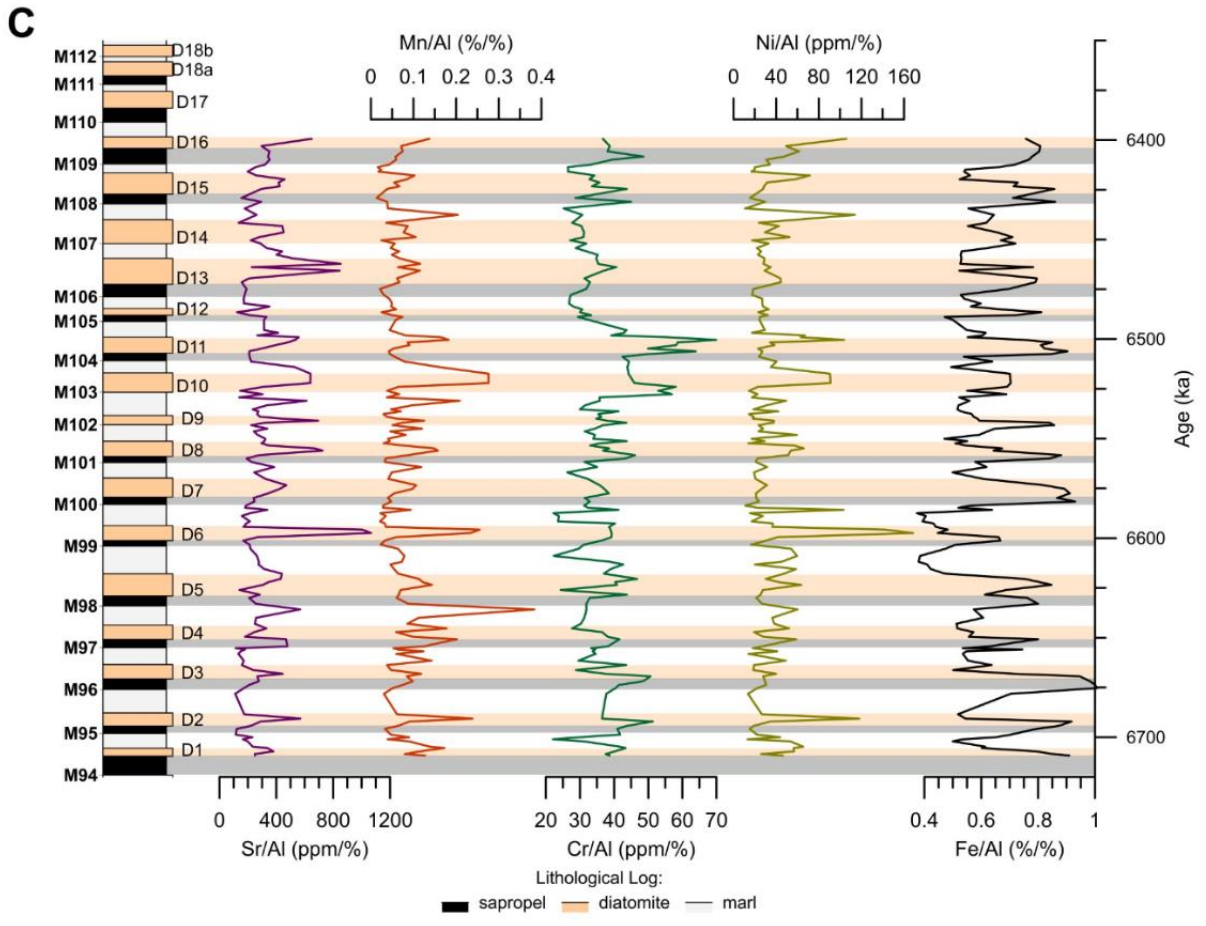

Figure 3 *(continued)*

is significantly higher than those for Pliocene sediments, which range from 0.011 to 0.016 (Wehausen and Brumsack, 2000). In most of the diatomites the P/Al ratio even exceeds 0.04, with a maximum of 0.09 at D6 (Fig. 3b).

The K/Al, Mg/Al, and Na/Al ratios display less clear patterns when compared to changes in lithology (Fig. 3b). However, similar to the Si/Al and Fe/Al ratios the K/Al ratio does present a clear alternating thin-thick cyclicity, related to the precession-obliquity interference pattern (Hilgen and Krijgsman, 1999). The K/Al ratio is moreover associated with the abundance of K-feldspar and illite (Wehausen and Brumsack, 2000; Calvert and Fontugne, 2001). The K/Al record also shows a decreasing trend from bottom to top (Fig. 3B). Sapropels appear to be characterized by high Na/Al values, but extremes seem to lack when a sapropel is missing and only a diatomite is present in the lithological record. High values of Mg/Al seem to correspond to sapropels and diatomites, whereas low values seem to correspond to homogenous marls. Elevated Mg/Al ratios can be explained by river-derived material from the north-western Aegean Sea originating from mafic/ultramafic rocks (Wehausen and Brumsack, 2000).

The ratios of redox-sensitive elements such as Sr/Al, Mn/Al, Cr/Al, Ni/Al, and Fe/Al display systematic enrichments within the sapropels compared to the background marls (Fig. 3c). Despite minor differences, the Sr/Al, Mn/Al, and Ni/Al records show a strong correlation and display relative depletions in the homogenous marls. Moreover, the Sr/Al pattern looks almost identical to the Ca/Al pattern, which could be due to the potential for geochemical substitution of these elements (e.g.: Lucas et al., 1990). Mn/Al ratios, conversely, have been used as an indicator for change in oxygenation levels (Wehausen and Brumsack, 2000; Calvert and Fontugne, 2001; Spofforth et al., 2008). In the Metochia section, sapropels are marked by relatively depleted Mn/Al values, while high Mn/Al values in the diatomites and homogenous marls could be the result of oxidation of Mn^{2+} in the sediment pore waters (or seawater) to MnO_x by increased bottom water O_2 levels, which becomes available at the end of sapropel formation (Thomson et al., 1993; Van Santvoort et al., 1996; Calvert and Pedersen, 2007). Similar to that of Mg, sources for Cr and Ni enriched material are the Greek rivers, which drain catchment areas with occurrences of ultramafic rocks. These rivers all discharge into the northwestern Aegean Sea and, by following per under with modern-day circulation patterns in the eastern Mediterranean, material from this region can reach the location of Gavdos (Wehausen and Brumsack, 2000).

4.2 Fe/Ti as a tracer of orbital forcing

Initially, this thesis aimed to use the Ti/Al ratio to investigate the tidal dissipation values of the late Messinian, as this ratio has been used successfully as an African monsoon proxy because of its more linear relationship (Lourens et al., 2001). However, based on the geochemical results of this study it was decided to use the Fe/Ti ratio rather than the Ti/Al ratio. Variations in C_{org}, Ba/Al and redox-sensitive elements may reflect a higher degree of non-linear response to the monsoonal forcing as they are sensitive to oceanic processes. Fe is also considered a redox-sensitive element, yet the Fe/Al pattern displays a more linear relation to insolation forcing compared to the other proxies (Figs. 3a, 4a). Yet, both the Fe/Al and Ti/Al records show a relative depression in values around 6.6 Ma. Alternative

for the use of Al as the element for detrital aluminosilicate normalization the Fe content can also be normalized to Ti to correct for variations in density and dust input. This results in a much better fit with the 65° N insolation curve of the La2004 solution compared to the Fe/Al and Ti/Al records (R^2 = 0.6351; Laskar et al., 2004). As described in the previous section, enrichments of the Fe content in sapropels could be attributed to detrital input and/or the formation of pyrite (FeS_2), which cause the increase in the Fe/Ti ratio over the assumed constant Fe/Ti detrital value (Thomson et al., 2008). The use of this Fe/Ti ratio eliminates the depression observed at 6.6 Ma.

The strong positive correlation (R_2 = 0.9438) of Ti and Al furthermore suggests that these elements react in a geochemically similar way and both are thus associated with terrigenous material (Fig. 4b). On the contrary, the poor correlation of Fe and Al (R_2 = 0.5822) could therefore exhibit a different depositional mechanism (i.e.: pyrite formation). Figure 4b presents moreover several clusters that represent the three different lithological units of the Metochia section. As can be expected, the highest Fe contents (2 – 4%) are associated with the sapropels, whereas the homogenous marls are specifically more associated with a higher Al content (up to 4.75 %). Although the diatomites contain a similar Fe content compared to the homogenous marls (1 – 2.5 %) they are marked by a relatively lower Al content. The highest Ti content is naturally observed in the homogenous marls (0.15 – 0.28 %), related to the enhanced dust input into the

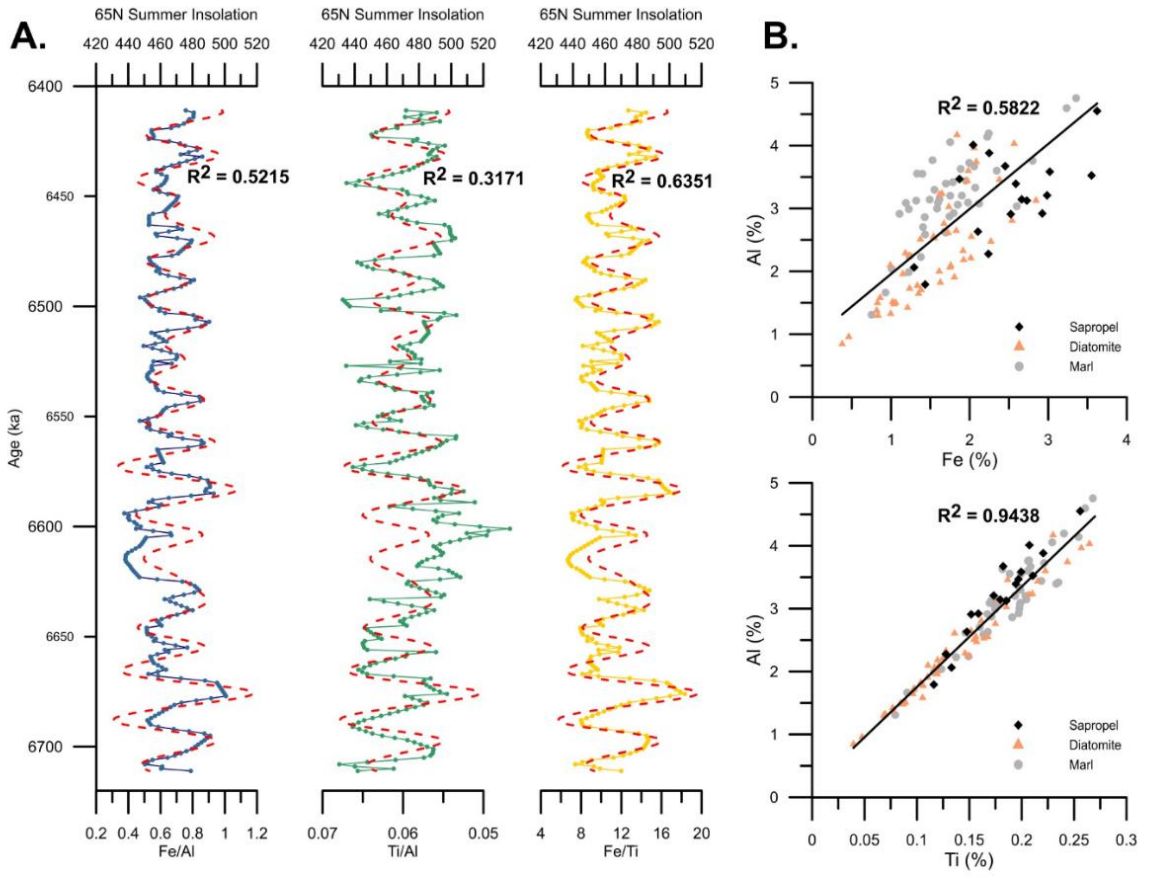

Fig. 4. A) The Fe/Al (blue), Ti/Al (green), and Fe/Ti (yellow) records plotted on top of the 65N summer insolation curve of the La2001$_{(1,1)}$ (red dotted line). **B**) Cross-plots showing the correlations of Fe vs. Al and Ti vs. Al. Pearson correlation coefficients (R^2) are also given (bold).

Mediterranean (Lourens et al., 2001). The distribution patterns of the Ti content of the sapropels and diatomites are less straightforward, despite that the sapropels appear to have a slightly higher Al content compared to the diatomites. The diatomites appear to exhibit overall relatively lower Al and Ti contents, which can be the consequence of dilution caused by the diatom blooms.

4.3 Astronomical tuning

A correct tuning between the proxy data and the astronomical solution is crucial for investigating changing values of Td and dE. Figure 5 shows the Fe/Ti proxy data and its filtered orbital frequencies as well as the filtered orbital frequencies of the 65°N insolation record of the La2001$_{(1,1)}$ astronomical solution. Despite some minor differences in amplitude the precession filters provide an excellent fit; no significant phase lags or mismatches can be observed (Fig. 5). The combined effect of the precession and obliquity frequencies provides a good correlation with the insolation curve of the La2001 solution with present-day values of Td and dE. Especially in the older part of the record (6.7 – 6.55 Ma) the two prominent peaks at 6.675 and 6.58 Ma, as well as the peaks surrounding these maxima, suggest that the tuning used for this study is correct. The broad peak at 6.625 Ma, resulting from the precession and obliquity interference, suggest a correct tuning. A different tuning would shift each cycle (at least) to one cycle older or younger. Consequently, those prominent peaks would correlate to less expressed cycles, which would result in a poor fit between proxy data and the astronomical solution.

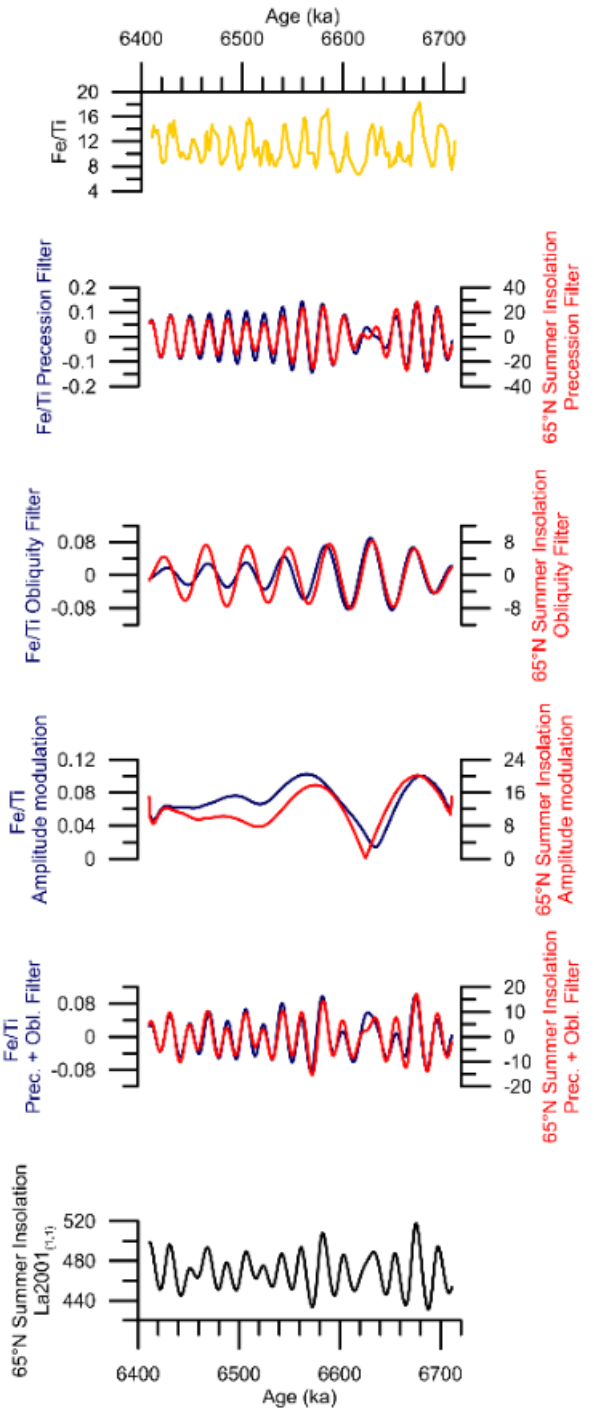

Fig. 5. Comparison between the filtered orbital frequencies of the time series for Fe/Ti and 65°N summer insolation derived from solution La2001$_{(1,1)}$. From top to bottom: the Fe/Ti record (yellow), the precession filters for the Fe/Ti record (dark blue) and the 65°N summer insolation record (red), the obliquity filters for the Fe/Ti record (dark blue) and the 65°N summer insolation record (red), the amplitude modulations of the precession filters for the Fe/Ti record (dark blue) and the 65°N summer insolation record (red), the merged precession and obliquity filters for the Fe/Ti record (dark blue) and the 65°N summer insolation record (red), and, the 65°N summer insolation derived from solution La2001$_{(1,1)}$ (black).

4.4 Late Messinian tidal dissipation values

The Fe/Ti proxy data traces the precession-obliquity interference pattern in the target curves well and displays a sinusoidal pattern (Figs. 4; 6). Figure 6a shows the Fe/Ti data plotted on top of the insolation curves of the La2001 astronomical solutions with varying values for Td. Although the insolation look similar for varying Td values, small differences in the amplitude of precession, as well as, changes in the precession-obliquity interference pattern already show minor inconsistencies between the Fe/Ti proxy data and the solutions. In particular, the La2001$_{(1,0.1)}$ solution displays inconstancies in amplitude variations compared to the Fe/Ti data at 6.66 and 6.53 Ma relative to the other solutions (Fig. 5a). By just visual comparison, the La2001$_{(1,0.9)}$ and La2001$_{(1,1.1)}$ solutions provide a relatively better fit compared to the La2001$_{(1,0.1)}$ and La2001$_{(1,0.5)}$ solutions. This is supported by figure 5b that shows (almost) identical phase lags in the precession band for the La2001$_{(1,0.1)}$ and La2001$_{(1,1.1)}$ solutions, especially for the 21-kyr band, which should be a logical result because the proxy data was tuned to the precession cycles. On the contrary, an offset of almost ~60° (~6.8 kyr) exists between both solutions in the obliquity band (Fig. 6b). Moreover, the

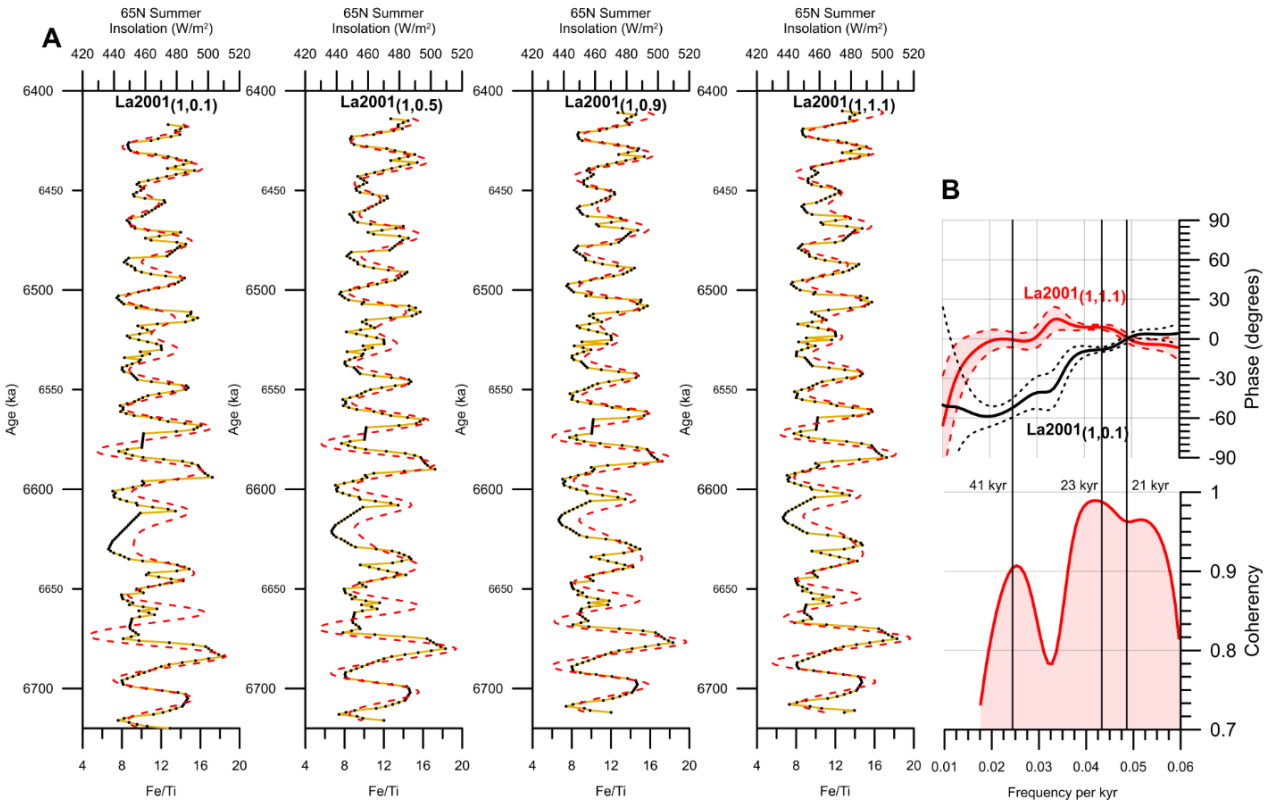

Fig. 6. Examples of cross-spectra between the Fe/Ti record and the La2001$_{(1,1)}$ 65°N summer insolation record. **A)** Comparison between the 1-kyr interpolated Fe/Ti timeseries (yellow) and the 65°N summer insolation timeseries (red dashed line) derived from the La2001 solution, with dE kept constant at 1 and Td values of 0.1, 0.5, 0.9, and 1.1 as indicated at the top of the plots (bold). **B)** Top panel: phase spectrum (degrees) between the time series for Fe/Ti and 65°N summer insolation derived from solutions La2001$_{(1,0.1)}$ (black) and La2001$_{(1,1.1)}$ (red). Dashed lines indicate lower and upper confidence limits at the 97.5% level that are given by: 0.399262 < ΔP (97.5%)/P < 4.937814. Lower panel: coherency spectrum between the time series for Fe/Ti and 65°N summer insolation derived from solution La2001$_{(1,1.1)}$.

coherency between the Fe/Ti proxy data and the La2001$_{(1,1.1)}$ solution is high (> 0.9) for both the precession and obliquity bands. Because of the tuning the geological data is, similar to the orbital target curves, dominated by the frequencies of precession. As a consequence, the obliquity component is able to keep its original phase relative to the different tuning targets (Lourens et al., 2001; Zeeden et al., 2014).

The tuned Fe/Ti record is compared with the 65°N insolation curve for the La2001 solutions with Td values varying between 0.0 and 1.2 (using steps of 0.1). The relationship between the regression coefficients and the obliquity-related phase lags can be described by a third-order polynomial curve (Fig. 7). This comparison shows that the optimum fit between Fe/Ti and the 65°N insolation curve is accomplished for the La2001$_{(1,1.1)}$ solution (Td = 1.1; Fig. 7). The obliquity-related time lag is -0.06 kyr ± 0.71 kyr, which approximates the phase lag related to precession (0.183 kyr ± 0.2 kyr). However, within the 97.5% confidence intervals, values of 1.2 and 1.0 also provide an in-phase relationship with obliquity and, therefore, cannot be statistically distinguished. Despite the larger obliquity lag, the solution with a Td value of 0.9 exhibits a good correlation coefficient (>0.64). The La2001 solutions with Td values deviating from these values resulted in relatively large obliquity phase lags. An out of phase relation with obliquity is inconstant with the assumption of direct climate response to insolation forcing for sapropels and are, therefore, not used for the determination of phase lags in section 4.6.

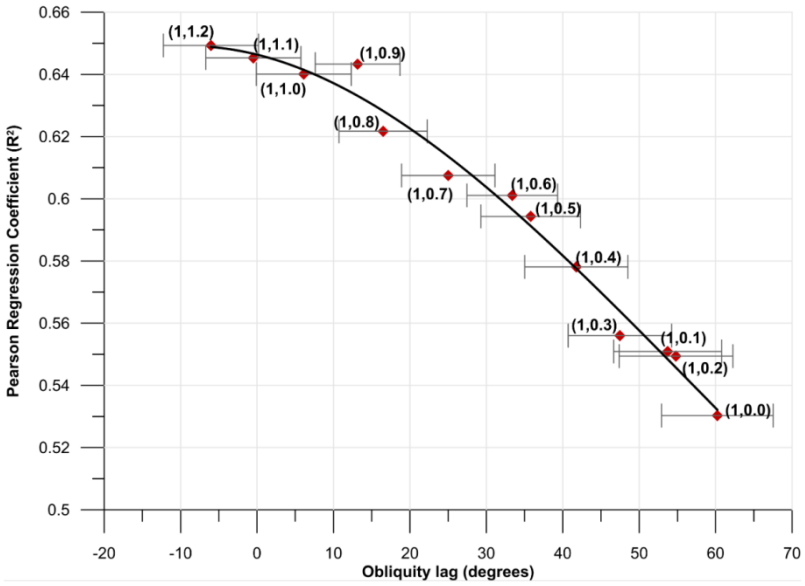

Fig. 7. Plot of the squared Pearson correlation coefficient (R_2) vs. the obliquity phase (degrees) of all investigated tunings. Error bars indicate the lower and upper confidence limits at the 97.5% level for the averaged obliquity phase lags (38-45 kyr). The Td value used for every data point is included.

4.5 Phase relations between the elemental ratios and precession and obliquity

The La2001$_{(1,1.1)}$ solution provided an excellent fit with the Fe/Ti data and, therefore, this solution was used to investigate phase lag relations relative to precession and obliquity for the other elemental ratios (Fig. 8). An in-phase relation between the Fe/Ti data and insolation forcing was used for the tuning to the target curves, which naturally results in a very high

coherency (>98%), as well as, (almost) no phase lag for the Fe/Ti record (Fig. 8a). In addition, a near 0° phase lag to obliquity was already observed for the Fe/Ti record in the previous section (Figs. 7, 8b).

Most striking is the similar ~60° (~3.5 kyr) phase lag relative to precession minima of the Ba/Al, Si/Al, and C_{org} records (fig. 8a), which may be related to the diatomite formation. Moreover, the Ba/Al and Si/Al records display a high coherency (>80%) with precession, while C_{org} shows a relatively poor coherency (60%) with the 65°N insolation record. This could therefore indicate deficiencies in the determination of the C_{org} content based on the TGA. A 195° phase lag (~11.3 kyr) and strong coherency was obtained for the Ti/Al record, which was expected as Ti/Al maxima occurred in the homogenous marls that were assumed to form during precession maxima (Figs. 3, 8a). An out-of-phase relation with precession is likewise obtained for the $CaCO_3$ and Zr/Al records, despite the phase lag being shorter compared to that of Ti/Al (150 and 160°, or, 8.75 and 9.3 kyr; Fig. 8a) It must also be noted that the obtained coherency of the $CaCO_3$ record with the insolation curve is poor compared to that of the Ti/Al and Zr/Al records. Furthermore, the Mn/Al, Ni/Al, P/Al, and Sr/Al records appear to be clustered and show a 90 to 110° phase lag to precession minima (5.3 to 6.4 kyr), while for the P/Al record the highest coherency (>90%) was established. The Cr/Al record also exhibits a high coherency (~90%) and displays a similar phase lag to Na/Al (~35 - 40°). The lowest value for coherency (~20%) with the 65°N insolation record was obtained for the Mg/Al record, while it also has an indistinct 270° phase lag, or 90° phase lead, relative to

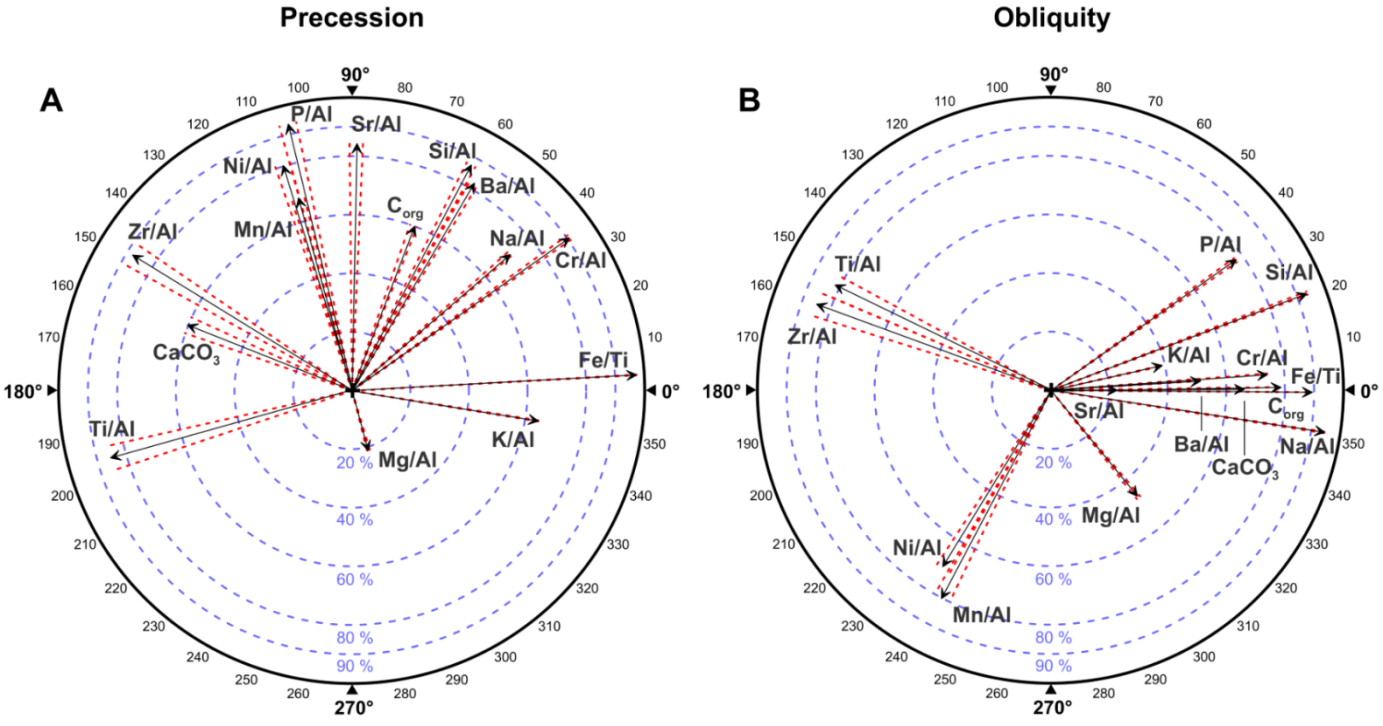

Fig. 8. Phase wheel diagrams for all elemental ratios showing **A)** the precession-related phase lags and **B)** obliquity-related phase lags from 0 to 360°. Note that a 0° phase lag represents an in-phase relation with insolation maxima; thus with precession minima and/or obliquity maxima. The length of the black arrow indicates the associated coherency between the elemental ratio and the 65°N insolation record of the $La2001_{(1,1.1)}$ astronomical solution as is indicated by the blue dashed circles (20 – 90%). The outer circle (black) represents here a 100% coherency. Coherencies are multiplied by 100 to be illustrated as percentages (%). Red dashed lines represent the lower and upper confidence limits at the 97.5% level for the averaged precession (18-25 kyr) and obliquity (38-45 kyr) phase lags.

precession. A 350° phase lag, or 10° phase lead, was established for the K/Al record, but this ratio also provides a poor coherency (~60%) with the insolation record.

Similar to Fe/Ti, the Sr/Al, Cr/Al, Ba/Al, C_{org}, and $CaCO_3$ records reveal a (almost) in-phase relation with obliquity (fig. 8b). However, large differences in the coherencies exist for these elemental ratios. The highest coherencies are obtained by the Fe/Ti, C_{org}, and Cr/Al records, in which the coherencies of the Fe/Ti and Cr/Al records have decreased slightly as compared to the coherencies with precession. On contrast, the coherency between obliquity and the C_{org} record has increased almost 20% compared to the coherency with precession (Fig. 8). Although the Ba/Al and Sr/Al records are in phase with obliquity they display a relatively poor coherency. A non-linear response of the Ba/Al record to obliquity could account for this poor coherency (Fig. 3b). It is remarkable that while Ba/Al, Si/Al, and C_{org} show a similar phase lag to precession, Si/Al shows a significant different phase lag to obliquity compared to Ba/Al and C_{org} (Fig. 8). The Si/Al record shows a phase lag of approximately 20° (~2.37 kyr) which is over 1 kyr longer than the phase lag observed to precession. Furthermore, of all elemental ratios besides Na/Al, the Si/Al record has the highest coherence with obliquity (Fig. 8b). As mentioned in section 4.1, the Si/Al record displays an alternating thin-thick pattern that is attributed to the precession-obliquity interference. Hence, a high coherency with obliquity could have been expected. The P/Al record shows a 35° (4.15 kyr) phase lag, whereas the Mn/Al and Ni/Al records show a -117° (28.8 kyr) and -121° (28.3 kyr) phase lag to obliquity respectively. The Ti/Al and Zr/Al records again show an almost anti-phase relation with insolation maxima (154° and 161°, or, 18.25 kyr and 19.08 kyr respectively), while these records show moreover a similar coherency with the insolation record when compared to precession (~85 %). A poor coherency (~45%) with the 65°N insolation record is again obtained for the Mg/Al record.

5. Discussion

5.1 Results of this study

The sediment samples from the Metochia section do differ in composition (high % Ca and low % Si) from the samples that are normally used and on which the XRF measuring method is based and calibrated. After XRF measurements, the sum of all measured elements was calculated. This resulted in sums just above 100% for samples with relatively high Ca content (mostly marls) after the XRF measurements, whereas other samples provided sums between 98 and 100%. Consequently, all XRF results were normalized to 100% to circumvent this problem. Normalization of the XRF data did not result in significant differences as all samples provided sums near 100%.

Furthermore, it must be noted that lithium borate fluxes volatize when heated at temperatures above 1050 °C, which could lead to inaccuracies of approximately 2-5% for the pre-fused flux used in this study (Loubser et al., 2004). The use of pre-used fluxes with different compositions would not have prevented this problem as all different compositions show a weight loss of more than 2% above 1020 °C. It is uncertain whether the calibration standard used for XRF measurements of this study accounted for lithium borate flux volatilization. Nonetheless, the XRF results do not appear to have been significantly affected by such volatilization and, therefore, it is not expected to affect the outcome of this study.

5.2 Arid/pluvial cycles in the deep marine Metochia sediments

The monsoonal variability is best displayed in the Fe/Al, Ti/Al, and Si/Al records. These proxies are moreover most related to changes in lithology. The behaviour of Fe in sapropels can be attributed to detrital input and/or redox state (Nijenhuis et al., 1996; Wehausen and Brumsack, 2000). The high Fe/Al ratios (> 0.6) in the sapropels are typical for euxinic conditions in deep basins (Canfield et al., 1996; Raiswell and Canfield, 1998; Lyons and Severmann, 2006; Scheiderich et al., 2010) and reflect transport of Fe^{2+} from adjacent suboxic parts of the basin to sulfidic basin regions (Lyons and Severmann, 2006). The anoxic/euxinic conditions that occur at times of sapropel formation are moreover indicated by depleted Mn/Al ratios (Fig. 3c). Due to reducing conditions and the Fe transport described above dissolution of Mn minerals occurs, which results in transportation of released Mn to the (sub)oxic surface waters and, therefore, in the deposition of Mn oxides at the shelves (Force and Cannon, 1988). The low Fe/Al ratios (~0.4 - 0.55) in the majority of the homogenous marls illustrate that Fe remobilization seems unlikely to have occurred. This is supported by the phase lag between the response of Fe/Al and Mn/Al to precession (Fig. 8a). The Mn/Al record displays a phase lag of almost 110° (~6.4 kyr) relative to that of Fe/Al. However, in some homogenous marl layers, Fe/Al peaks correspond with peaks in Mn/Al, indicating the possibility of remobilized Fe and Mn as the result of early diagenesis (Figs. 3a, 3c; Van Santvoort et al., 1996). These intervals coincide moreover with enrichments in Ni/Al ratios (Fig. 3c), and could therefore indicate that diagenetic processes are most likely to dominate the signal in these marls (e.g. in the marls overlying diatomites D6, D10, D13, and D14; Köhler et al., 2008).

Dissolved Fe is believed to be connected to primary productivity, since Fe is a limiting nutrient and stimulates cyanobacterial N_2-fixation (Sañudo-Wilhelmy et al., 2001; Mills et al., 2004; Saltzman, 2005). Additionally, at times of sapropel formation, the release of P from Fe-oxides beneath suboxic stratified waters can result in a high biotic response when upwelling is initiated (Stratford et al., 2000). This could furthermore stimulate productivity as P is also considered a key nutrient (Van Cappellen and Ingall, 1994).When the stored excess phosphorus is exhausted it results in the deposition of homogenous marls that are marked by decreased productivity (Filippelli et al., 2003). Enrichments in the P/Al ratio are, however, predominantly observed in the diatomaceous layers (Fig. 3b).

Wehausen and Brumsack (1998) showed that enriched Ba concentrations in the sapropels are related to higher rates of primary production. The Ba/Al, P/Al, and C_{org} records show a similar phase lag to precession, indicating that these proxies are related to the same mechanism; productivity (Fig. 8a). However, enrichments in Ba/Al, P/Al, and C_{org} occur predominantly in the diatomites of the Metochia section, rather than in the sapropels (Fig. 3a). It is therefore expected that the enriched Fe/Al ratios are most likely related to anoxic/euxinic conditions, whereas the diatomites resemble periods of increased productivity. Results from this study do show C_{org} content above 2%, but so do most of the homogenous marls (Fig. 3a). It must thus be noted that no direct measurements of C_{org} have been implemented in this study and C_{org} contents are solely based on estimates from the TGA, which introduces some uncertainties in the interpretation of the C_{org} record. Nonetheless, sapropels are commonly associated with increased C_{org} export from the surface waters and consequent O_2 consumption and the dark colour suggests relatively high contents of organic matter. Hence, more direct

measurements of the C_{org} content, quantification of the V content (Thomson et al., 1995), or the use of Br/Al as Total Organic Carbon (TOC) proxy (Ziegler et al., 2008) could further improve the results of this study.

The source of Fe in the sapropels and diatomites comes from the enhanced detrital input of Fe-bearing smectite minerals (Foucault and Méliéres, 2000; Wehausen and Brumsack, 2000). The African summer monsoon drives the hydrologic budget in the Eastern Mediterranean during precession minima/insolation (Marzocchi et al., 2019). Maximum precipitation reached the eastern Mediterranean via the Nile, as well as Miocene paleochannels, which flowed through present-day Libya to the Gulf of Sirte draining a more humid Sahara (Griffin, 2002, 2006; Paillou et al., 2009; 2012; Ghoneim et al., 2012). During these humid periods, an increase in fluvial erosion provided an increased terrigenous supply to marine sedimentation (Foucault and Méliéres, 2000). High smectite contents have been recorded in Messinian sediments in the Lake Chad and Lake Cyrenaica areas, as well as, in the Nile delta (Moussa et al., 2016; Leila, 2019). The Fe content could, therefore, trace the variability of the ferromagnesian minerals that should reflect the pyroxene and smectite contents in the Blue Nile sediments (Foucault and Stanley, 1989), which are derived from the weathering of Ethiopian basalts (El-Anwar and Samy, 2013). Additionally, increased smectite mineral contents entered the Mediterranean Sea via northern African river systems at times of insolation maxima (Griffin 2002, 2006). The role of these (paleo-)drainage areas in contributing to the enhanced run-off into the Mediterranean are consistent with climate models that suggest that the combined monsoonal run-off contributions of the Sahel and Sahara regions are needed to obtain an in-phase relation with climatic precession (Simon et al., 2017; De Boer et al., 2021). Enhanced runoff during precession minima is moreover consistent with spikes in productivity, water column stratification, and sapropel formation (Rohling, 1994; Matthiesen and Haines, 2003). Water column stratification is furthermore supported by the high Zr/Al ratios in the homogenous marls of the Metochia section (Fig. 3a). These enrichments point to particle sorting and therefore may indicate stronger water currents (Bahr et al., 2014; Kaboth et al., 2015), whereas depleted Zr/Al ratios in the sapropels may indicate more stagnant conditions, or, the presence of more angular grains associated with aeolian sediments (Konijnendijk et al., 2014). The Zr/Al record has a precessional phase lag of 150° (~8.75 kyr) and is thus (almost) in anti-phase with precession (Fig. 8), similar to the Ti/Al ratio, which suggests that the Zr/Al ratio is most likely affected by aeolian dust input rather than by water currents.

The combined effect of the fluvial Fe-input and anoxic/euxinic bottom water conditions is most likely the source for Fe-enrichments in the sapropels and diatomites. During insolation maxima, monsoonal run-off delivered high amounts of Fe to the Mediterranean where the oxygen-depleted bottom waters provided the ideal circumstances for the precipitation of Fe in the form of pyrite. The presence and distribution of pyrite in the sediments could have been demonstrated by the means of sulphur distribution patterns (Calvert and Fontugne, 2001), however, sulphur compositions were not determined for this study as that required another set of measurements and calibration methods. Furthermore, anoxic bottom water conditions during sapropel formation could have been indicated by the sulphur isotopic composition of pyrite in the sapropels (Passier et al., 1999; Scheiderich et al., 2010), yet those measurements were beyond the scope of this thesis.

Aridity in northern Africa can best be described by the Ti/Al proxy (Lourens et al., 2001; Larrasoana et al., 2003). Lourens et al. (2001) showed that the Ti/Al ratio in the Pliocene sediments from ODP Site 967 in the eastern Mediterranean provided an excellent fit with the P-1/2t curve and it was suggested to reflect humid/arid climate variability. High Ti/Al values in the homogenous marls indicate a more arid climate during deposition, while low Ti/Al values in the sapropels and diatomites indicate a more humid climate during deposition. Although the average Ti/Al ratios in the Metochia sediments are in the same range as for Pliocene sapropels (Wehausen and Brumsack, 2000; Lourens et al., 2001), a clear linear relationship between the proxy and insolation record, as seen in Lourens et al. (2001), is lacking. Reduced aeolian dust input could result in the observation of decreased Ti content in the homogenous marls from the Metochia section. Alternatively, increased Al input from the Aegean region could also lower the ratio (*see fig. 14*: Wehausen and Brumsack, 2000). When the Aegean input into the Mediterranean dominates the terrigenous input, the higher contribution of Al will lower the Ti/Al ratio so that it is no longer a suitable proxy for aeolian dust input. Yet, the Ti/Al ratio can be associated with aeolian dust derived from North Africa when the Aegean terrigenous contribution is limited. However, Köhler et al. (2008) showed that the Aegean terrigenous contribution in the Metochia section decreased rapidly at ~8.2 Ma, while at the same time North Africa was predominantly controlled by a relatively humid

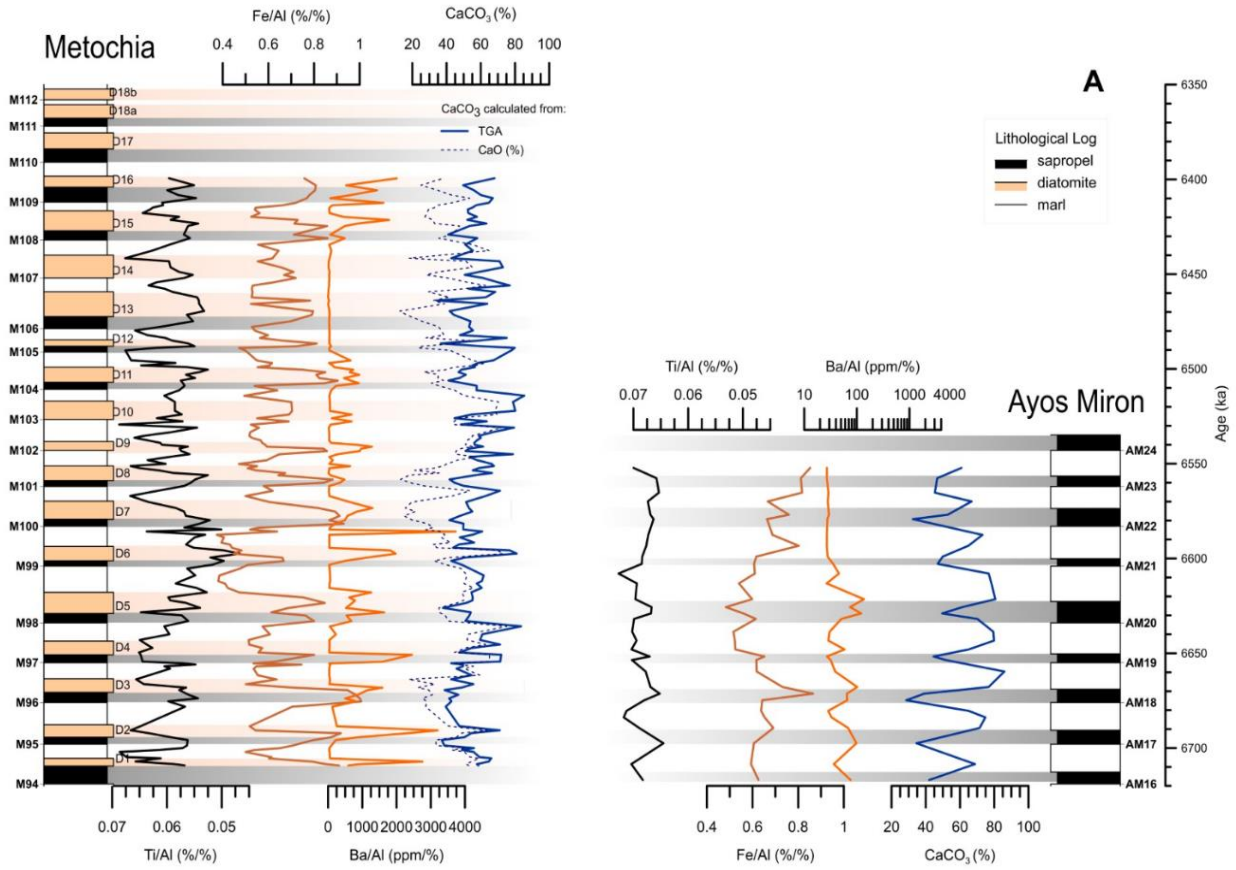

Fig. 9. Selected elemental ratios for the Metochia section (left) and the Ayos Miron section (right) plotted on a timescale (6.72 – 6.4 Ma). The lithological logs of both sections are also plotted, with numbered Metochia cylces (M94-M112) and numberd Ayos Miron cycles (AM16 – AM24). Diatomitee cycles of the Metochia section are also plotted on the right side of the log (D1-D18b). The lithological log is also plotted on the background, where the grey bars represent sapropels, light orange bars represent diatomites, and white bars represent homogenous marls. Note that the x-axes for Ba/Al and Mn/Al for the Ayos Miron section are plotted on a log scale in order to visualize elemental variability while still using identical axes values as for the Metochia section.

climate. The presence of humid conditions in the Late Miocene is also recorded in several offshore sediment cores as they record low dust fluxes from North Africa (e.g.: Colin et al., 2014). These conditions could also explain the relatively lower values for Ti/Al maxima (<0.07) compared to those from the Pliocene at ODP Site 967 (0.8; Lourens et al., 2001).

Furthermore, the Ti/Al ratio in the Metochia sediments is in anti-phase with precession minima/insolation maxima, whereas phase lags of other elements related to Aegean run-off (e.g.: Cr, K, Mg, Ni; Wehausen and Brumsack, 2000) differ significantly (Fig. 8a). It is here, therefore, suggested that Ti is primarily of aeolian origin and can be used as proxy for aridity. Although the record of Köhler et al. (2008) is limited to 7.2 Ma, it is expected that for the time interval of this study (6.7 – 6.4 Ma) the terrigenous input remains also limited. However, one clear exception could be observed in the Fe/Al and Ti/Al proxy records at 6.6 Ma (Fig 4). This interval displays low Fe/Al values (indicative for relatively arid conditions) as well as relatively low Ti/Al values (indicative for relatively humid conditions), which cannot be explained other than that those signals are the result of an increased input of Al. This depression is significantly decreased when the Fe content is divided by the Ti content, which moreover justifies the use of Fe/Ti as a reliable proxy for humid versus arid conditions in North Africa to investigate Messinian values for Td in this study (Fig. 4).

5.3 Comparison with the Ayos Miron section (Crete)

Selected elemental ratios have been compared to those of the Ayos Miron section (Crete; Fig. 9). The Ayos Miron section is located at approximately 50 km from the Metochia section, yet significant differences in the elemental ratio patterns can be observed. The Ayos Miron section was located at a depth of 400 – 700 m during the Messinian, while the Metochia section was located in deep waters around 1200 m (van Hinsbergen and Meulenkamp, 2006). The phase relation between Ti/Al to insolation maxima is similar for both sites, since both sections display high Ti/Al ratios during marl depositon and decreased Ti/Al ratios during sapropel formation. However, the observed anomaly around 6.6 Ma due to enhanced Aegean Al-input is less evident for the Ayos Miron section. On the contrary, the record from the Ayos Miron shows high Ti/Al ratios and thus relatively arid conditions at 6.62 Ma (Fig. 9a). This could possibly the result of different water sources reaching the sites, although this seems unlikely as the Ayos Miron section is located closer to the Aegean main land compared to the Gavdos section. While the Fe/Al ratio is enriched in the Metochia sapropels (and diatomites), the Fe/Al ratio in the Ayos Miron section shows a less strong signal, which could be due to increased oxygen levels at the site of the shallower Ayos Miron section. The Mn/Al ratio in the Ayos Miron section does, however, indicate anoxic conditons at times of sapropel formation (Fig. 9b). Absolute Mn/Al values are significantly lower in the sediments of the Ayos Miron section compared to those in the Metochia sediments. Yet, it must be noted that elemental concentrations for the Ayos Miron sediments were determined using LA-ICP while elemental concentrations in this study were determined using XRF. If both locations had similar anoxic conditions the difference in Fe/Al patterns could be explained by the transport of Fe into the Mediterranean. It could be that Fe-bearing smectite minerals originating from northern Africa could reach the deep waters at the Metochia section, but could not reach the shallower site of the Ayos Miron section. This reasoning can moreover explain the difference

in average Fe/Al ratios observed for these locations; ~0.7 for Metochia and ~0.6 for Ayios Miron.

The $CaCO_3$ content differs significantly between these locations, although it must be noted that $CaCO_3$ in this study is, like the C_{org} content measured indirectly. The calcium carbonate content in the Ayos Miron section shows a nice cyclicity related to its lithology, whereas the Metochia record displays a more distorted signal. Increased terrigenous input is likely to have resulted in high productivity at this location, as indicated by the Ba/Al and P/Al proxies. Such conditions, (e.g. high fresh-water runoff) could have favoured siliceous productivity over carbonate productivity, whereas the Ayos Miron section was more dominated by carbonate productivity (Taylforth et al., 2014). Considerable differences exist between the P/Al records of both locations. In general, both records show P/Al enrichments just after sapropel formation, or, insolation maxima. Considerable differences thus exist between the two sites, despite their close distance, and it is, therefore, suggested that elemental concentrations in the deep marine sediments of the Metochia section was primarily controlled by influences from the south, whereas the shallower marine sediments from the Ayos Miron section were predominantly controlled by carbonate production and, possibly, by northern river systems from the Aegean mainland.

5.4 Comparison of past tidal dissipation values

The $La2001_{(1,1.1)}$ solution gives the best and most significant fit with the Fe/Ti proxy record, although this result may be statistically indistinguishable from the $La2001_{(1.1)}$ and $La2001_{(1,1.2)}$ solutions (Fig. 6); it is therefore suggested to use a maximum range from 1.05 to

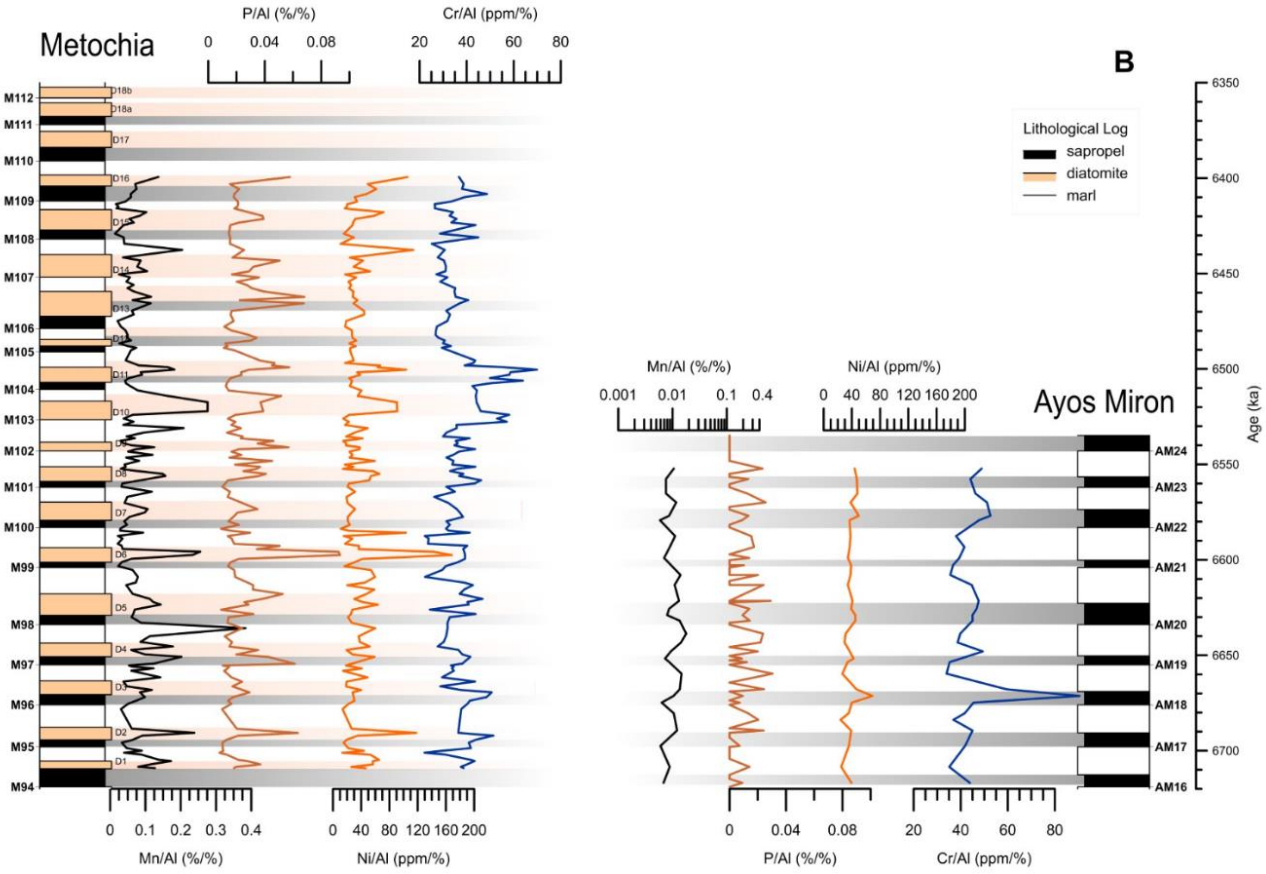

Figure 10 (continued)

1.15 for Td. This result is consistent with the Td value of ~1 established for the Miocene at the 9–9.6, 11.5–12.1, and 12.1 – 12.5 Ma time intervals in the Monte dei Corvi section (Hüsing et al., 2007; Zeeden et al., 2014). Zeeden et al. (2014) also obtained high correlation coefficients and relatively consistent obliquity phases for Td values of 0.3–0.5 that originated from a tuning that was shifted one precession cycle to achieve a good fit between their proxy data and the orbital solution. For the younger interval (6.7 Ma – 6.4 Ma) of this study, it was not necessary to implement a shift of one precession cycle to obtain a good fit between proxy data and the astronomical solutions (Fig. 5). For example, a one precession cycle shift in the Fe/Ti proxy data would by contrast result in major inconsistencies in precession-obliquity interference patterns as well as in precessional amplitude patterns between the proxy data and 65°N insolation record of the $La2001_{(1,0.5)}$ astronomical solution (Fig. 5). Moreover, Hüsing et al. (2007) found, based on visual comparison of the cycle patterns, that a present-day Td value (1,1) provided no convincing match, whereas a Td value of 1.2 obtained the best fit with the cycle patterns. This implied that a Td value larger than the present-day value is needed to obtain the best fit between proxy data and the astronomical solution for the Miocene, which is in agreement with the 1.05 – 1.15 Td obtained in this study.

Results from this study are also consistent with Td values obtained for the last 3 million years (Lourens et al., 2001). However, despite that Lourens et al. (2001) concluded that the present-day values for Td and dE in the La90 solution (Laskar, 1990) resulted in a good match, an optimum fit between their proxy data and the La90 solution was actually obtained using a Td value of 0.5. As mentioned in Zeeden et al. (2014), the obtained 0.5 Td value could be associated to changes in dE associated with the Northern Hemisphere glaciations, since only the combined effect of Td and dE can be investigated (Laskar et al., 1993; Mitrovica et al., 1994; Morrow et al., 2012). No further conclusions can be made regarding this statement as only varying Td values have been investigated in this study. Pälike and Shackleton (2000) did investigate the change both Td and dE values in their study, which complicates the comparison with our study. They argued, however, that these parameters have remained close to the present-day values over the last 25 million years and it does, therefore, not contradict the outcome of this study.

On the contrary, Green et al. (2017) argued that past values for Td must have been much lower than present-day values, much like the 0.5 Td obtained by Lourens et al. (2001) as well as the 0.4 Td obtained by Zeeden et al. (2014) by shifting the tuning one precession cycle. They found that the total globally integrated dissipation rate for the Miocene was 50% of the degraded model present rate, which was mainly explained by a narrower Atlantic ocean during the Miocene relative to present-day. However, it was also shown that the tidal dissipation rates in the abyssal ocean were enhanced due to more energy being lost in the deep ocean in the Miocene case than at present (*Fig. 4 in* Green et al., 2017).

Furthermore, a Td value of 1.05 – 1.15 implies a constant and direct response of African climate changes to insolation, which is consistent with transient climate modelling experiments that imply no precession- and obliquity-related time lags for the African monsoon and Miocene sapropels (Ziegler et al., 2010; Weber and Tuenter, 2011; Simon et al., 2017; De Boer et al., 2021). For late Pleistocene a ~3 kyr phase lag is often assumed, however, Ziegler et al. (2010) demonstrated that such a phase lag could be the result of a

delay of the African monsoon to insolation forcing due to the occurrence of cold events in the North Atlantic, which are not known to occur during warmer Miocene.
At last, compared to the $La2001_{(1,1.1)}$ solution, the phase lags for the $La2004_{(1,1)}$ solution are -2.12 ± 0.03 kyr for precession and -2.04 ± for 0.07 kyr for obliquity, which should be taken into account when investigating phase relations between proxy data and astronomical forcing in the Messinian when using the La2004 solution. This (un)certainty limits the precision of determining phase relations but moreover improves the understanding of the limitations of tuned time scales and determining phase relations that have been performed for the Messinian.

5.5 Implications of the precession-related phase lag on the Mediterranean diatomites

The proxies for productivity (e.g: Ba/Al, C_{org}, and P/Al; Figs. 3a, 3b, 8) in the results of this study are related to the deposition of the diatomaceous layers. The diatomites display a precession-related time lag of ~60°, or ~3.5 kyr, to the 65°N insolation record of the $La2001_{(1,1.1)}$ solution (Fig. 8). This phase lag is similar to the phase lag of 3.3 kyr ± 2.6 kyr obtained for the Messinian gypsum deposits based on a simple box model, in which the lag is attributed to salinity changes and vertical mixing in the Mediterranean (Topper and Meijer, 2015). Similar phase lags have been observed between Sr-isotope anomalies and vertical mixing of the water column and the hydrological budget in the Sorbas basin (Modestou et al., 2017).

Traditionally, the diatomites are interpreted as evidence of the gradually restricted conditions that characterized the Mediterranean just before the Messinian salinity crisis. However, their coeval occurrence with a global intensification of the opaline production in the world oceans (late Miocene-early Pliocene biogenic bloom) suggests a causal relationship between sapropel and diatomite deposition in the Mediterranean, considering the possible interplay between stratification-adapted diatoms and anaerobic bacteria (Pellegrino et al., 2018). During precession minima, a strong run-off provided huge amounts of dissolved Si to the Mediterranean derived by the leaching of grassland soils and promoted water column stratification, which favoured the proliferation of oligospecific, highly silicified subsurface diatom assemblages (Pellegrino et al., 2018). Upon reaching the seafloor, the diatom frustules were dissolved due to the activity of sulphate-reducing bacteria (SRB) which increased alkalinity of the pore waters. By contrast, during more arid phases, the reduction of monsoonal runoff and the mixing of the water column favoured the re-injection of recycled dissolved Si in the photic layer that was previously trapped below the pycnocline. Phytolith-rich dust further contributed to the silica saturation of the water column. Diversified diatom assemblages, adapted to exploit the silica-rich surface waters, proliferated and their frustules were further deposited on the oxygenated sea bottom. The suppression of sulphate-reducing bacteria favoured the preservation of diatom frustules.

This model of diatomite deposition, as proposed by Pellegrino et al. (2018), is consistent with the idea of precession-related phase of salinity changes and vertical mixing. If the diatomite deposition is thus initiated by changes in vertical mixing during more arid periods, after insolation maxima and sapropel formation, it could be argued that the phase lag obtained in this study is also the result of such changes. Although diatomite deposition is more accentuated in the western domain than in the central and eastern domains (Hilgen and

Krijgsman, 1999; Pérez-Folgado et al., 2003), they could be (in part) isochronous in both basins (Filippelli et al., 2003). If so, the precession-related phase lags for the diatomites of the Metochia section could be identical for the diatomites found in the western Mediterranean, despite that the western Mediterranean and the Atlantic margin are also influenced by enhanced winter precipitation from the Atlantic storm tracks (Marzocchi et al., 2019).

The determination of precession-related phase lags for the diatomites in the western Mediterranean could be of importance to the astronomical tuning of the Sorbas basin (Spain; Sierro et al., 2001). The astronomical tuning of the Abad section was transferred to an open marine succession from the Messinian Melilla section in Morocco, using planktonic foraminiferal events (van Assen et al., 2006), since the Melilla section lacked the sedimentary cycles that contain the expression of characteristic details related to precession amplitude and precession-obliquity interference that are common in Mediterranean sapropel sequences (Krijgsman et al., 1999). Astronomical ages were then assigned to intercalated tephra layers, which allowed for the intercalibration of astronomical ages and $^{40}Ar/^{39}Ar$ dated sanidine phenocrysts, and this resulted in an unprecedentedly precise age for the Fish Canyon sanidine (28.201 ± 0.023 Ma; Kuiper et al., 2008). However, consensus about the age of 28.201 ± 0.023 Ma from Kuiper et al. (2008) is still lacking in the literature (Channell et al. 2010; Renne et al. 2010; Rivera et al. 2011).

Absolutely crucial for the proposed intercalibration of the $^{40}Ar/^{39}Ar$ dating method and the astronomical method is an absolutely perfect analysis of cyclicity, or, a correct astronomical tuning. Phase lags between climate and climate proxies have implications for the appropriate location of astronomical tuning tie points within each orbital cycle. It has been argued that tuning of the Abad marls by tying precession minima to the midpoint of sapropelic layers is incorrect as sapropelic layers were deposited during the transition to precession minima, rather than being centred symmetrically around it (Pérez-Folgado et al., 2003). Modestou et al. (2017) proposed that the tuning for the Abad section could be evaluated, or possibly improved, by tuning the diatomites to precession maxima. However, based on the results here it is suggested to tune the diatomites to precession minima using the precession-related phase lag observed in this study (~3.5 kyr). While this is beyond the scope of this study it could be part of future research. This could have implications for the intercalibration between the astronomical ages and $^{40}Ar/^{39}Ar$ ages used for the age determination of the Fish Canyon sanidine. It remains, however, uncertain if the maximum change in the astronomical age would result in a significant different age that was not yet incorporated in the uncertainties of ash layer ages by Kuiper et al. (2008) and Rivera et al. (2011). Moreover, the discrepancies of reported ages for $^{40}Ar/^{39}Ar$ dating standards relative to the ones intercalibrated (Channell et al., 2010; Renne et al., 2010) with astronomical time scales (Kuiper et al., 2008; Rivera et al., 2011) can probably not be attributed to the effect of Td and dE, since these discrepancies encompass one or multiple precession cycles (Zeeden et al., 2014).

6. Conclusions

The Messinian Metochia section (6.72 – 6.4 Ma) contains intricate cycle patterns in the XRF proxy data related to orbitally induced climate change. The sapropels of the Metochia section were deposited during periods of enhanced precipitation over North Africa, which

resulted in the increased input of Fe-bearing smectite minerals into the Mediterranean via Miocene paleochannels and the river Nile. Deposition of Fe then occurred in the anoxic bottom waters of the eastern Mediterranean. Conversely, the homogenous marls of the Metochia section were deposited during relatively arid periods, resulting in a relative increase of aeolian Ti input. Together this allowed for the use of Fe/Ti as proxy for humid versus arid conditions in northern Africa and this ratio was used to investigate Messinian tidal dissipation values. The Fe/Ti data provided an optimum fit with the 65° insolation record of the La2001 solution with a Td value of ~1.1, indicating that this value is the most accurate from a geological point of view**.** This value is, however, statically indistinguishable to that of the $La2001_{(1,1.2)}$ and $La2001_{(1,1)}$ solutions. The data presented here contributes moreover to the determination of the accuracy of phase relations between insolation forcing and climate response during the late Miocene. Astronomical tunings and determinations of phase relations that have previously been determined for Messinian climate data should implement a -2.12 ± 0.03 kyr phase lag for precession and a -2.04 ± for 0.07 kyr for obliquity, since the $La2004_{(1,1)}$ solution lags the $La2001_{(1,1.1)}$. An additional precession-related phase lag of ~3.5 kyr was established for the diatomites of the Metochia section, which could have implications for the tuning of other Mediterranean diatomites.

Acknowledgements

I would like to thank my supervisors Prof. Dr. Lucas J. Lourens and Dr. F.J. Hilgen for their great help and support during this study. For technical assistance in the lab I am grateful to Jan van Tongeren.

References

Assen, E. van, K. F. Kuiper, N. Barhoun, W. Krijgsman, and F. J. Sierro. 2006. "Messinian Astrochronology of the Melilla Basin: Stepwise Restriction of the Mediterranean-Atlantic Connection through Morocco." *Palaeogeography, Palaeoclimatology, Palaeoecology* 238 (1–4): 15–31. https://doi.org/10.1016/j.palaeo.2006.03.014.

Bahr, André, Francisco J. Jiménez-Espejo, Nada Kolasinac, Patrick Grunert, F. Javier Hernández-Molina, Ursula Röhl, Antje H.L. Voelker, et al. 2014. "Deciphering Bottom Current Velocity and Paleoclimate Signals from Contourite Deposits in the Gulf of Cádiz during the Last 140 Kyr: An Inorganic Geochemical Approach." *Geochemistry, Geophysics, Geosystems* 15 (8): 3145–60. https://doi.org/10.1002/2014GC005356.

Barboni, Melanie, Patrick Boehnke, Brenhin Keller, Issaku E. Kohl, Blair Schoene, Edward D. Young, and Kevin D. McKeegan. 2017. "Early Formation of the Moon 4.51 Billion Years Ago." *Science Advances* 3 (1): 1–9. https://doi.org/10.1126/sciadv.1602365.

Boer, Bas De, Marit Peters, and Lucas J. Lourens. 2021. "The Transient Impact of the African Monsoon on Plio-Pleistocene Mediterranean Sediments." *Climate of the Past* 17 (1): 331–44. https://doi.org/10.5194/cp-17-331-2021.

Bosmans, J. H.C., F. J. Hilgen, E. Tuenter, and L. J. Lourens. 2015. "Obliquity Forcing of Low-Latitude Climate." *Climate of the Past* 11 (10): 1335–46. https://doi.org/10.5194/cp-11-1335-2015.

Calvert, S E, and M R Fontugne. 2001. "On the Late Pleistocene-Holocene Sapropel Record of Climatic and Oceanographic Variability in the Eastern Mediterranean." *Paleoceanography* 16 (1): 78–94. https://doi.org/10.1029/1999PA000488.

Calvert, S E, and T F Pedersen. 2007. "Elemental Proxies for Palaeoclimatic and Palaeoceanographic Variability in Marine Sediments: Interpretation and Application." In *Developments in Marine Geology*, 568–625. Elsevier B.V. https://doi.org/10.1016/S1572-5480(07)01019-6 r.

Canfield, Donald E., Timothy W. Lyons, and Robert Raiswell. 1996. "A Model for Iron Deposition to Euxinic Black Sea Sediments." *American Journal of Science*. https://doi.org/10.2475/ajs.296.7.818.

Cappellen, Philippe Van, and Ellery D. Ingall. 1994. "Benthic Phosphorus Regeneration, Net Primary Production, and Ocean Anoxia: A Model of the Coupled Marine Biogeochemical Cycles of Carbon and Phosphorus." *Paleoceanography* 9 (5): 677–92. https://doi.org/10.1029/94PA01455.

Channell, J. E.T., D A Hodell, B S Singer, and C Xuan. 2010. "Reconciling Astrochronological and 40Ar/39Ar Ages for the Matuyama-Brunhes Boundary and Late Matuyama Chron." *Geochemistry, Geophysics, Geosystems* 11 (12): 0–12. https://doi.org/10.1029/2010GC003203.

Colin, Christophe, Giuseppe Siani, Zhifei Liu, Dominique Blamart, Charlotte Skonieczny, Yulong Zhao, Aloys Bory, et al. 2014. "Late Miocene to Early Pliocene Climate Variability off NW Africa (ODP Site 659)." *Palaeogeography,*

Palaeoclimatology, Palaeoecology 401: 81–95. https://doi.org/10.1016/j.palaeo.2014.02.015.
Coulthard, Tom J., Jorge A. Ramirez, Nick Barton, Mike Rogerson, and Tim Brücher. 2013. "Were Rivers Flowing across the Sahara during the Last Interglacial? Implications for Human Migration through Africa." *PloS One* 8 (9). https://doi.org/10.1371/journal.pone.0074834.
Drinia, Hara, Assimina Antonarakou, Nikolaos Tsaparas, and George Kontakiotis. 2007. "Palaeoenvironmental Conditions Preceding the Messinian Salinity Crisis: A Case Study from Gavdos Island." *Geobios* 40 (3): 251–65. https://doi.org/10.1016/j.geobios.2007.02.003.
El-Anwar, E A, and Y Samy. 2013. "Clay Mineralogy and Geochemical Characterization of Some Quaternary Sediments on Giza-Fayium District, Western Side of the Nile Valley, Egypt: Relationships to Weathering and Provenance." *Australian Journal of Basic and Applied Sciences* 7 (6): 754–69.
Filippelli, Gabriel M., F. J. Sierro, J. A. Flores, A. Vázquez, R. Utrilla, M. Pérez-Folgado, and J. C. Latimer. 2003. "A Sediment-Nutrient-Oxygen Feedback Responsible for Productivity Variations in Late Miocene Sapropel Sequences of the Western Mediterranean." *Palaeogeography, Palaeoclimatology, Palaeoecology* 190: 335–48. https://doi.org/10.1016/S0031-0182(02)00613-2.
Force, E. R., and W. F. Cannon. 1988. "Depositional Model for Shallow- Marine Manganese Deposits around Black Shale Basins." *Economic Geology* 83 (1): 93–117. https://doi.org/10.2113/gsecongeo.83.1.93.
Foucault, Alain, and Frédèric Méliéres. 2000. "Palaeoclimatic Cyclicity in Central Mediterranean Pliocene Sediments: The Mineralogical Signal." *Palaeogeography, Palaeoclimatology, Palaeoecology* 158 (3–4): 311–23. https://doi.org/10.1016/S0031-0182(00)00056-0.
Foucault, Alain, and Daniel Jean Stanley. 1989. "Late Quaternary Palaeoclimatic Oscillations in East Africa Recorded by Heavy Minerals in the Nile Delta." *Nature* 339 (6219): 44–46. https://doi.org/10.1038/339044a0.
Ghoneim, Eman, Michael Benedetti, and Farouk El-Baz. 2012. "An Integrated Remote Sensing and GIS Analysis of the Kufrah Paleoriver, Eastern Sahara." *Geomorphology* 139–140: 242–57. https://doi.org/10.1016/j.geomorph.2011.10.025.
Gradstein, Felix M., James G. Ogg, and Frits J. Hilgen. 2012. "On the Geologic Time Scale." *Newsletters on Stratigraphy* 45 (2): 171–88. https://doi.org/10.1127/0078-0421/2012/0020.
Gradstein, Felix M., James G. Ogg, Alan G. Smith, Wouter Bleeker, and Lucas J. Lourens. 2004. "A New Geologic Time Scale, with Special Reference to Precambrian and Neogene." *Episodes* 27 (2): 83–100. https://doi.org/10.18814/epiiugs/2004/v27i2/002.
Green, J. A.M., and M. Huber. 2013. "Tidal Dissipation in the Early Eocene and Implications for Ocean Mixing." *Geophysical Research Letters* 40 (11): 2707–13. https://doi.org/10.1002/grl.50510.
Green, J. A.M., M. Huber, D. Waltham, J. Buzan, and M. Wells. 2017. "Explicitly Modelled Deep-Time Tidal Dissipation and Its Implication for Lunar History." *Earth and Planetary Science Letters* 461: 46–53. https://doi.org/10.1016/j.epsl.2016.12.038.
Griffin, David L. 2002. "Aridity and Humidity: Two Aspects of the Late Miocene Climate of North Africa and the Mediterranean." *Palaeogeography, Palaeoclimatology, Palaeoecology* 182 (1–2): 65–91. https://doi.org/10.1016/S0031-0182(01)00453-9.
Griffin, David L.. 2006. "The Late Neogene Sahabi Rivers of the Sahara and Their Climatic and Environmental Implications for the Chad Basin." *Journal of the Geological Society* 163 (6): 905–21. https://doi.org/10.1144/0016-76492005-049.
Guieu, C., and A. Thomas. 1996. *Saharan Aerosol: From the Soil to the Ocean*. *The Impact of Desert Dust across the Mediterranean, Edited by S. Guerzoni and R. Chester*. Kluwer Acad., Dordrecht, Netherlands. https://doi.org/doi:10.1007/978-94-017–3354-0_20.
Hansen, Kirk S. 1982. "Secular Effects of Oceanic Tidal Dissipation on the Moon's Orbit and the Earth's Rotation." *Reviews of Geophysics* 20 (3): 457–80. https://doi.org/10.1029/RG020i003p00457.
Haven, H. L. Ten, M. Baas, J. W. De Leeuw, P. A. Schenck, and H. Brinkhuis. 1987. "Late Quaternary Mediterranean Sapropels II. Organic Geochemistry and Palynology of S1 Sapropels and Associated Sediments." *Chemical Geology* 64 (1–2): 149–67. https://doi.org/10.1016/0009-2541(87)90160-4.
Hilgen, F. J., W. Krijgsman, C. G. Langereis, L. J. Lourens, A. Santarelli, and W. J. Zachariasse. 1995. "Extending the Astronomical (Polarity) Time Scale into the Miocene." *Earth and Planetary Science Letters* 136 (3–4): 495–510. https://doi.org/10.1016/0012-821X(95)00207-S.
Hilgen, Frederik J., and Wout Krijgsman. 1999. "Cyclostratigraphy and Astrochronology of the Tripoli Diatomite Formation (Pre-Evaporite Messinian, Sicily, Italy)." *Terra Nova* 11 (1): 16–22. https://doi.org/10.1046/j.1365-3121.1999.00221.x.
Hilgen, Frederik J., Lucas J. Lourens, Jan A. Van Dam, Alan G. Beu, Andrew F. Boyes, Roger A. Cooper, Wout Krijgsman, James G. Ogg, Werner E. Piller, and Douglas S. Wilson. 2012. *The Neogene Period*. *The Geologic Time Scale 2012*. Elsevier. https://doi.org/10.1016/B978-0-444-59425-9.00029-9.
Hinsbergen, Douwe J.J. van, and Johan E. Meulenkamp. 2006. "Neogene Supradetachment Basin Development on Crete (Greece) during Exhumation of the South Aegean Core Complex." *Basin Research* 18 (1): 103–24. https://doi.org/10.1111/j.1365-2117.2005.00282.x.
Hüsing, S. K., F. J. Hilgen, H. Abdul Aziz, and W. Krijgsman. 2007. "Completing the Neogene Geological Time Scale between 8.5 and 12.5 Ma." *Earth and Planetary Science Letters* 253 (3–4): 340–58. https://doi.org/10.1016/j.epsl.2006.10.036.
Jimenez-Espejo, F. J., F. Martinez-Ruiz, M. Rogerson, J. M. González-Donoso, O. E. Romero, D. Linares, T. Sakamoto, et al. 2008. "Detrital Input, Productivity Fluctuations, and Water Mass Circulation in the Westernmost Mediterranean Sea since the Last Glacial Maximum." *Geochemistry, Geophysics, Geosystems* 9 (11). https://doi.org/10.1029/2008GC002096.
Kaboth, Stefanie, André Bahr, Gert Jan Reichart, Bram Jacobs, and Lucas J Lourens. 2015. "New Insights into Upper MOW

Variability over the Last 150 Kyr from IODP 339 Site U1386 in the Gulf of Cadiz." *Marine Geology* 377: 136–45. https://doi.org/10.1016/j.margeo.2015.08.014.
Köhler, C. M., D. Heslop, M. J. Dekkers, W. Krijgsman, D. J.J. Van Hinsbergen, and T. Von Dobeneck. 2008. "Tracking Provenance Change during the Late Miocene in the Eastern Mediterranean Using Geochemical and Environmental Magnetic Parameters." *Geochemistry, Geophysics, Geosystems* 9 (12): 1–14. https://doi.org/10.1029/2008GC002127.
Konijnendijk, T. Y.M., M Ziegler, and L J Lourens. 2014. "Chronological Constraints on Pleistocene Sapropel Depositions from High-Resolution Geochemical Records of ODP Sites 967 and 968." *Newsletters on Stratigraphy* 47 (3): 263–82. https://doi.org/10.1127/0078-0421/2014/0047.
Krijgsman, W., F. J. Hilgen, I. Raffi, F. J. Sierro, and D. S. Wilson. 1999. "Chronology, Causes and Progression of the Messinian Salinity Crisis." *Nature* 400 (6745): 652–55. https://doi.org/10.1038/23231.
Krijgsman, W, F J Hilgen, C G Langereis, A Santarelli, and W J Zachariasse. 1995. "Late Miocene Magnetostratigraphy, Biostratigraphy and Cyclostratigraphy in the Mediterranean." *Earth and Planetary Science Letters* 136 (95): 475–94.
Kuiper, K F, A Deino, F J Hilgen, W Krijgsman, P R Renne, and J R Wijbrans. 2008. "Synchronizing Rock Clocks of Earth History." *Science* 320 (5875): 500–504. https://doi.org/10.1126/science.1154339.
Lange, Gert J. De, John Thomson, Anja Reitz, Caroline P. Slomp, M. Speranza Principato, Elisabetta Erba, and Cesare Corselli. 2008. "Synchronous Basin-Wide Formation and Redox-Controlled Preservation of a Mediterranean Sapropel." *Nature Geoscience* 1 (9): 606–10. https://doi.org/10.1038/ngeo283.
Larrasoana, J. C., A. P. Roberts, E. J. Rohling, M. Winklhofer, and R. Wehausen. 2003. "Three Million Years of Monsoon Variability over the Northern Sahara." *Climate Dynamics* 21 (7–8): 689–98. https://doi.org/10.1007/s00382-003-0355-z.
Laskar, J. 1990. "The Chaotic Motion of the Solar System: A Numerical Estimate of the Size of the Chaotic Zones." *Icarus* 88 (2): 266–91. https://doi.org/10.1016/0019-1035(90)90084-M.
Laskar, J., F. Joutel, and F. Boudin. 1993. "Orbital, Precessional, and Insolation Quantities for the Earth from -20Myr to +10Myr." *Astronomy and Astrophysics* 270 ((1-2)): 522–33.
Laskar, J, A Fienga, M Gastineau, and H Manche. 2011. "La2010: A New Orbital Solution for the Long-Term Motion of the Earth." *Astronomy and Astrophysics* 532: 89. https://doi.org/10.1051/0004-6361/201116836.
Laskar, J, P Robutel, F Joutel, M Gastineau, A. C.M. Correia, and B Levrard. 2004. "A Long-Term Numerical Solution for the Insolation Quantities of the Earth." *Astronomy and Astrophysics* 428 (1): 261–85. https://doi.org/10.1051/0004-6361:20041335.
Latimer, Jennifer C., and Gabriel M. Filippelli. 2001. "Terrigenous Input and Paleoproductivity in the Southern Ocean." *Paleoceanography* 16 (6): 627–43. https://doi.org/10.1029/2000PA000586.
Latimer, Jennifer C., and Gabriel M. Filippelli. 2002. "Eocene to Miocene Terrigenous Inputs and Export Production: Geochemical Evidence from ODP Leg 177, Site 1090." *Palaeogeography, Palaeoclimatology, Palaeoecology* 182 (3–4): 151–64. https://doi.org/10.1016/S0031-0182(01)00493-X.
Lee, Der Chuen, Alex N. Halliday, Gregory A. Snyder, and Lawrence A. Taylor. 1997. "Age and Origin of the Moon." *Science* 278 (5340): 1098–1103. https://doi.org/10.1126/science.278.5340.1098.
Leila, Mahmoud. 2019. "Clay Minerals Distribution in the Pre-, Syn-Messinian Salinity Crisis Sediments of the Onshore Nile Delta, Egypt: Mineral Origin and Implications on the Reservoir Quality." *Journal of African Earth Sciences* 154 (March): 35–48. https://doi.org/10.1016/j.jafrearsci.2019.03.016.
Loubser, Maggi, Christien Strydom, and Herman Potgieter. 2004. "A Thermogravimetric Analysis Study of Volatilization of Flux Mixtures Used in XRF Sample Preparation." In *X-Ray Spectrometry*, 33:212–15. https://doi.org/10.1002/xrs.700.
Lourens, L J, A Antonarakou, F J Hilgen, A A M Van Hoof, and W J Zachariasse. 1996. "Evaluation of the Plio-Pleistocene Astronomical Timescale Established to the Precession Time Series of the Astronomical Solution of Berger the Sedimentary Cycle Patterns with 65 ØN Summer Insolation Time Series Components in the 65 ØN Summer Insolation Cu." *Paleoceanography* 11 (4): 391–413. https://doi.org/10.1029/96PA01125.
Lourens, Lucas J. 2004. "Revised Tuning of Ocean Drilling Program Site 964 and KC01B (Mediterranean) and Implications for the Δ18O, Tephra, Calcareous Nannofossil, and Geomagnetic Reversal Chronologies of the Past 1.1 Myr." *Paleoceanography* 19 (3): 1–20. https://doi.org/10.1029/2003PA000997.
Lourens, Lucas J., Rolf Wehausen, and Hans J. Brumsack. 2001. "Geological Constraints on Tidal Dissipation and Dynamical Ellipticity of the Earth over the Past Three Million Years." *Nature* 409 (6823): 1029–33. https://doi.org/10.1038/35059062.
Lucas, J., E. M. El Faleh, and L. Prevot. 1990. "Experimental Study of the Substitution of Ca by Sr and Ba in Synthetic Apatites." *Phosphorite Research and Development*, no. 52: 33–47.
Lyons, Timothy W., and Silke Severmann. 2006. "A Critical Look at Iron Paleoredox Proxies: New Insights from Modern Euxinic Marine Basins." *Geochimica et Cosmochimica Acta* 70 (23 SPEC. ISS.): 5698–5722. https://doi.org/10.1016/j.gca.2006.08.021.
Marzocchi, Alice, Rachel Flecker, Daniel J. Lunt, Wout Krijgsman, and Frits J. Hilgen. 2019. "Precessional Drivers of Late Miocene Mediterranean Sedimentary Sequences: African Summer Monsoon and Atlantic Winter Storm Tracks." *Paleoceanography and Paleoclimatology* 34 (12): 1980–94. https://doi.org/10.1029/2019PA003721.
Matthiesen, Stephan, and Keith Haines. 2003. "A Hydraulic Box Model Study of the Mediterranean Response to Postglacial Sea-Level Rise." *Paleoceanography* 18 (4). https://doi.org/10.1029/2003PA000880.
Mills, Matthew M., Celine Ridame, Margaret Davey, Julie La Roche, and Richard J. Geider. 2004. "Iron and Phosphorus Co-Limit Nitrogen Fixation in the Eastern Tropical North Atlantic." *Nature* 429 (6989): 292–94. https://doi.org/10.1038/nature02550.
Mitrovica, J. X., Rongshi Pan, and A. M. Forte. 1994. "Late Pleistocene and Holocene Ice Mass Fluctuations and the Earth's Precession Constant." *Earth and Planetary Science Letters* 128 (3–4): 489–500. https://doi.org/10.1016/0012-821X(94)90165-1.

Modestou, Sevasti, Dirk Simon, Marcus Gutjahr, Alice Marzocchi, Tanja J. Kouwenhoven, Rob M. Ellam, and Rachel Flecker. 2017. "Precessional Variability of 87Sr/86Sr in the Late Miocene Sorbas Basin: An Interdisciplinary Study of Drivers of Interbasin Exchange." *Paleoceanography* 32 (6): 531–52. https://doi.org/10.1002/2016PA003061.

Morrow, E., J. X. Mitrovica, A. M. Forte, P. Glišović, and P. Huybers. 2012. "An Enigma in Estimates of the Earth's Dynamic Ellipticity." *Geophysical Journal International* 191 (3): 1129–34. https://doi.org/10.1111/j.1365-246X.2012.05703.x.

Moussa, Abderamane, Alice Novello, Anne Elisabeth Lebatard, Alain Decarreau, Claude Fontaine, Doris Barboni, Florence Sylvestre, et al. 2016. "Lake Chad Sedimentation and Environments during the Late Miocene and Pliocene: New Evidence from Mineralogy and Chemistry of the Bol Core Sediments." *Journal of African Earth Sciences* 118: 192–204. https://doi.org/10.1016/j.jafrearsci.2016.02.023.

Nijenhuis, I. A., S. J. Schenau, C. H. Van Der Weijden, F. J. Hilgen, L. J. Lourens, and W. J. Zachariasse. 1996. "On the Origin of Upper Miocene Sapropelites: A Case Study from the Faneromeni Section, Crete (Greece)." *Paleoceanography* 11 (5): 633–45. https://doi.org/10.1029/96PA01963.

Paillard, Didier, Laurent Labeyrie, and Pascal Yiou. 1996. "Macintosh Program Performs Time-Series Analysis." *Eos, Transactions American Geophysical Union* 77 (39): 379–379. https://doi.org/10.1029/96eo00259.

Paillou, Philippe, Mathieu Schuster, Stephen Tooth, Tom Farr, Ake Rosenqvist, Sylvia Lopez, and Jean Marie Malezieux. 2009. "Mapping of a Major Paleodrainage System in Eastern Libya Using Orbital Imaging Radar: The Kufrah River." *Earth and Planetary Science Letters* 277 (3–4): 327–33. https://doi.org/10.1016/j.epsl.2008.10.029.

Paillou, Philippe, Stephen Tooth, and Sylvia Lopez. 2012. "The Kufrah Paleodrainage System in Libya: A Past Connection to the Mediterranean Sea?" *Comptes Rendus - Geoscience* 344 (8): 406–14. https://doi.org/10.1016/j.crte.2012.07.002.

Pälike, Heiko, and Nicholas J. Shackleton. 2000. "Constraints on Astronomical Parameters from the Geological Record for the Last 25 Myr." *Earth and Planetary Science Letters* 182 (1): 1–14. https://doi.org/10.1016/S0012-821X(00)00229-6.

Passier, Hilde F., Jack J. Middelburg, Gert J. De Lange, and Michael E. Böttcher. 1999. "Modes of Sapropel Formation in the Eastern Mediterranean: Some Constraints Based on Pyrite Properties." *Marine Geology* 153 (1–4): 199–219. https://doi.org/10.1016/S0025-3227(98)00081-4.

Pearson, K. 1895. "Mathematical Contributions to the Theory of Evolution - III. Regression, Heredity, and Panmixia." *Philosophical Transactions of the Royal Society of London. Series A, Containing Papers of a Mathematical or Physical Character* 191: 229–311.

Pellegrino, Luca, Francesco Dela Pierre, Marcello Natalicchio, and Giorgio Carnevale. 2018. "The Messinian Diatomite Deposition in the Mediterranean Region and Its Relationships to the Global Silica Cycle." *Earth-Science Reviews* 178 (February): 154–76. https://doi.org/10.1016/j.earscirev.2018.01.018.

Raiswell, Robert, and Donald E. Canfield. 1998. "Sources of Iron for Pyrite Formation in Marine Sediments." *American Journal of Science* 298 (3): 219–45. https://doi.org/10.2475/ajs.298.3.219.

Reichart, Gert-Jan. 1997. *Late Quaternary Variability of the Arabian Sea Monsoon and Oxygen Minimum Zone*. *Geologica Ultraiectina*. Vol. 154.

Renne, Paul R., Roland Mundil, Greg Balco, Kyoungwon Min, and Kenneth R. Ludwig. 2010. "Joint Determination of 40K Decay Constants and 40Ar*/40K for the Fish Canyon Sanidine Standard, and Improved Accuracy for 40Ar/39Ar Geochronology." *Geochimica et Cosmochimica Acta* 74 (18): 5349–67. https://doi.org/10.1016/j.gca.2010.06.017.

Rivera, Tiffany A., Michael Storey, Christian Zeeden, Frederik J. Hilgen, and Klaudia Kuiper. 2011. "A Refined Astronomically Calibrated 40Ar/39Ar Age for Fish Canyon Sanidine." *Earth and Planetary Science Letters* 311 (3–4): 420–26. https://doi.org/10.1016/j.epsl.2011.09.017.

Rodrigo-Gámiz, M., F. Martínez-Ruiz, F. J. Jiménez-Espejo, D. Gallego-Torres, V. Nieto-Moreno, O. Romero, and D. Ariztegui. 2011. "Impact of Climate Variability in the Western Mediterranean during the Last 20,000 Years: Oceanic and Atmospheric Responses." *Quaternary Science Reviews* 30 (15–16): 2018–34. https://doi.org/10.1016/j.quascirev.2011.05.011.

Rohling, Eelco J. 1994. "Review and New Aspects Concerning the Formation of Eastern Mediterranean Sapropels." *Marine Geology* 122 (1–2): 1–28. https://doi.org/10.1016/0025-3227(94)90202-X.

Rossignol-Strick, Martine. 1985. "Mediterranean Quaternary Sapropels, an Immediate Response of the African Monsoon to Variation of Insolation." *Palaeogeography, Palaeoclimatology, Palaeoecology* 49 (3–4): 237–63. https://doi.org/10.1016/0031-0182(85)90056-2.

Saltzman, Matthew R. 2005. "Phosphorus, Nitrogen, and the Redox Evolution of the Paleozoic Oceans." *Geology* 33 (7): 573–76. https://doi.org/10.1130/G21535.1.

Santvoort, P. J.M. Van, G. J. De Lange, J. Thomson, H. Cussen, T. R.S. Wilson, M. D. Krom, and K. Ströhle. 1996. "Active Post-Depositional Oxidation of the Most Recent Sapropel (S1) in Sediments of the Eastern Mediterranean Sea." *Geochimica et Cosmochimica Acta* 60 (21): 4007–24. https://doi.org/10.1016/S0016-7037(96)00253-0.

Sañudo-Wilhelmy, Sergio A., Adam B. Kustka, Christopher J. Gobler, David A. Hutchins, Min Yang, Kamazima Lwiza, James Burns, Douglas G. Capone, John A. Raven, and Edward J. Carpenter. 2001. "Phosphorus Limitation of Nitrogen Fixation by Trichodesmium in the Central Atlantic Ocean." *Nature* 411 (6833): 66–69. https://doi.org/10.1038/35075041.

Scheiderich, K., A. L. Zerkle, G. R. Helz, J. Farquhar, and R. J. Walker. 2010. "Molybdenum Isotope, Multiple Sulfur Isotope, and Redox-Sensitive Element Behavior in Early Pleistocene Mediterranean Sapropels." *Chemical Geology* 279 (3–4): 134–44. https://doi.org/10.1016/j.chemgeo.2010.10.015.

Schenau, S. J., A. Antonarakou, F. J. Hilgen, L. J. Lourens, I. A. Nijenhuis, C. H. Van Der Weijden, and W. J. Zachariasse. 1999. "Organic-Rich Layers in the Metochia Section (Gavdos, Greece): Evidence for a Single Mechanism of Sapropel Formation during the Past 10 My." *Marine Geology* 153 (1–4): 117–35. https://doi.org/10.1016/S0025-3227(98)00086-3.

Sierro, F. J., F. J. Hilgen, W. Krijgsman, and J. A. Flores. 2001. “The Abad Composite (SE Spain): A Messinian Reference Section for the Mediterranean and the APTS.” *Palaeogeography, Palaeoclimatology, Palaeoecology* 168 (1–2): 141–69. https://doi.org/10.1016/S0031-0182(00)00253-4.

Simon, Dirk, Alice Marzocchi, Rachel Flecker, Daniel J. Lunt, Frits J. Hilgen, and Paul Th Meijer. 2017. “Quantifying the Mediterranean Freshwater Budget throughout the Late Miocene: New Implications for Sapropel Formation and the Messinian Salinity Crisis.” *Earth and Planetary Science Letters* 472: 25–37. https://doi.org/10.1016/j.epsl.2017.05.013.

Sonett, Author C P, E P Kvale, A Zakharian, Marjorie A Chan, T M Demko, C P Sonett, E P Kvale, A Zakharian, Marjorie A Chan, and T M Demko. 1996. “Late Proterozoic and Paleozoic Tides , Retreat of the Moon , and Rotation of the Earth Published by : American Association for the Advancement of Science Stable URL : Https://Www.Jstor.Org/Stable/2890055 American Association for the Advancement of Science.” *Science* 273 (5271): 100–104.

Spofforth, David J.A., Heiko Pälike, and Darryl Green. 2008. “Paleogene Record of Elemental Concentrations in Sediments from the Arctic Ocean Obtained by XRF Analyses.” *Paleoceanography* 23 (1): 1–13. https://doi.org/10.1029/2007PA001489.

Stratford, K., R.G. Williams, and P.G. Myers. 2000. “Impact of the Circulation on Sapropel Formation in the Eastern Mediterranean.” *Global Biogeochemical Cycles* 14 (2): 683–95. https://doi.org/10.1016/S0025-3227(99)00093-6.

Taylforth, Joseph E, Gillian A. McCay, Rob Ellam, Isabella Raffi, Dick Kroon, and Alastair H.F. Robertson. 2014. “Middle Miocene (Langhian) Sapropel Formation in the Easternmost Mediterranean Deep-Water Basin: Evidence from Northern Cyprus.” *Marine and Petroleum Geology* 57: 521–36. https://doi.org/10.1016/j.marpetgeo.2014.04.015.

Thomson, J., I. W. Croudace, and R. G. Rothwell. 2008. “A Geochemical Application of the ITRAX Scanner to a Sediment Core Containing Eastern Mediterranean Sapropel Units.” *Geological Society, London, Special Publications* 267 (1): 65–77. https://doi.org/10.1144/gsl.sp.2006.267.01.05.

Thomson, J., N. C. Higgs, I. W. Croudace, S. Colley, and D. J. Hydes. 1993. “Redox Zonation of Elements at an Oxic/Post-Oxic Boundary in Deep-Sea Sediments.” *Geochimica et Cosmochimica Acta* 57 (3): 579–95. https://doi.org/10.1016/0016-7037(93)90369-8.

Thomson, J., N. C. Higgs, T. R.S. Wilson, I. W. Croudace, G. J. De Lange, and P. J.M. Van Santvoort. 1995. “Redistribution and Geochemical Behaviour of Redox-Sensitive Elements around S1, the Most Recent Eastern Mediterranean Sapropel.” *Geochimica et Cosmochimica Acta* 59 (17): 3487–3501. https://doi.org/10.1016/0016-7037(95)00232-O.

Topper, R. P.M., and P. Th Meijer. 2015. “The Precessional Phase Lag of Messinian Gypsum Deposition in Mediterranean Marginal Basins.” *Palaeogeography, Palaeoclimatology, Palaeoecology* 417: 6–16. https://doi.org/10.1016/j.palaeo.2014.10.025.

Tuenter, E., S. L. Weber, F. J. Hilgen, and L. J. Lourens. 2003. “The Response of the African Summer Monsoon to Remote and Local Forcing Due to Precession and Obliquity.” *Global and Planetary Change* 36 (4): 219–35. https://doi.org/10.1016/S0921-8181(02)00196-0.

Weber, S. L., and E. Tuenter. 2011. “The Impact of Varying Ice Sheets and Greenhouse Gases on the Intensity and Timing of Boreal Summer Monsoons.” *Quaternary Science Reviews* 30 (3–4): 469–79. https://doi.org/10.1016/j.quascirev.2010.12.009.

Wehausen, R., and H. J. Brumsack. 1998. “The Formation of Pliocene Mediterranean Sapropels: Constraints from High-Resolution Major and Minor Element Studies.” *Proceedings of the Ocean Drilling Program: Scientific Results* 160: 207–18. https://doi.org/10.2973/odp.proc.sr.160.004.1998.

Wehausen, R, and H. J. Brumsack. 1999. “Cyclic Variations in the Chemical Composition of Eastern Mediterranean Pliocene Sediments: A Key for Understanding Sapropel Formation.” *Marine Geology* 153 (1–4): 161–76. https://doi.org/10.1016/S0025-3227(98)00083-8.

Wehausen, Rolf, and Hans Jürgen Brumsack. 2000. “Chemical Cycles in Pliocene Sapropel-Bearing and Sapropel-Barren Eastern Mediterranean Sediments.” *Palaeogeography, Palaeoclimatology, Palaeoecology* 158 (3–4): 325–52. https://doi.org/10.1016/S0031-0182(00)00057-2.

Wehausen, Rolf, and Hans Jürgen Brumsack. 2002. “Astronomical Forcing of the East Asian Monsoon Mirrored by the Composition of Pliocene South China Sea Sediments.” *Earth and Planetary Science Letters* 201 (3–4): 621–36. https://doi.org/10.1016/S0012-821X(02)00746-X.

Westerhold, Thomas, Ursula Röhl, and Jacques Laskar. 2012. “Time Scale Controversy: Accurate Orbital Calibration of the Early Paleogene.” *Geochemistry, Geophysics, Geosystems* 13 (6). https://doi.org/10.1029/2012GC004096.

Williams, George E. 2000. “Geological Constraints on the Precambrian History of Earth’s Rotation and the Moon’s Orbit.” *Reviews of Geophysics* 38 (1): 37–59. https://doi.org/10.1029/1999RG900016.

Zeeden, Christian, Frederik J. Hilgen, Silja K. Hüsing, and Lucas L. Lourens. 2014. “The Miocene Astronomical Time Scale 9-12-Ma: New Constraints on Tidal Dissipation and Their Implications for Paleoclimatic Investigations.” *Paleoceanography* 29 (4): 296–307. https://doi.org/10.1002/2014PA002615.

Ziegler, M., T. Jilbert, G.J. De Lange, L.J. Lourens, and G.J. Reichart. 2008. “Bromine Counts from XRF Scanning as an Estimate of the Marine Organic Carbon Content of Sediment Cores.” *Geochemistry, Geophysics, Geosystems* 9 (5): 1–6. https://doi.org/10.1029/2007GC001932.

Ziegler, Martin, Lucas J. Lourens, Erik Tuenter, Frits Hilgen, Gert Jan Reichart, and Nanne Weber. 2010. “Precession Phasing Offset between Indian Summer Monsoon and Arabian Sea Productivity Linked to Changes in Atlantic Overturning Circulation.” *Paleoceanography* 25 (3): 1–16. https://doi.org/10.1029/2009PA001884.